

ANALYSIS OF STRAIN ACCUMULATION OF THE FAULTING ZONES  
BY THE HELP OF CONTINUOUS GPS STATIONS

by

Asude ARSLAN

B.S. Geodesy and Photogrametry Engineering, in Yıldız Technical University, 2004



Submitted to the Kandilli Observatory and Earthquake  
Research Institute in partial fulfillment of  
the requirements for the degree of  
Master of Science

Graduate Program in Geodesy

Boğaziçi University

2007

## LIST OF FIGURES

Figure 1.1.	The distribution of continuous (MAGNET, TUGENET) and campaign GPS sites .....	2
Figure 2.1.	Simplified tectonic map of the Eastern Mediterranean with zones of coherent motion .....	3
Figure 2.2.	Surface ruptures and cumulative slips along NAFZ. ....	4
Figure 2.3.	Similarity between North Anatolian and San Andreas Faults.....	5
Figure 2.4.	Distribution of active faults in the Anatolian region.....	6
Figure 2.5.	The Marmara region showing the mapped faults .....	7
Figure 2.6.	Updated GPS velocities near the Marmara Sea region.....	8
Figure 2.7.	Mapped faults and GPS vectors referenced to fixed Anatolia.....	9
Figure 2.8.	Historical seismicity of the Marmara Region .....	10
Figure 3.1.	The geometric problem of 3-D positioning from ranges.....	12
Figure 3.2.	Flow chart of GIPSY process .....	15
Figure 3.3.	GPS Points used in this study .....	19
Figure 3.4.	Displacements of stations between 2002 and 2004.....	20
Figure 4.1.	Three kinds of differential stress.....	23
Figure 4.2.	Homogeneous strain .....	25

Figure 4.3.	Heterogeneous strain.....	25
Figure 4.4.	The blue cube is rotated in a clockwise direction about the z-axis.....	27
Figure 4.5.	The green cube is translated parallel to the x-axis.....	27
Figure 4.6.	The purple cube is being distorted or strained.....	27
Figure 4.7.	Length Deformation.....	28
Figure 4.8.	Stretch figure.....	29
Figure 4.9.	Volume Deformation.....	30
Figure 4.10.	Angular strain.....	30
Figure 4.11.	Shear strain.....	31
Figure 4.12.	Simple shear.....	31
Figure 4.13.	The translation of point a is used to illustrate the mathematics of pure shear.....	32
Figure 4.14.	Elastic Deformation.....	33
Figure 4.15.	Brittle Failure.....	33
Figure 4.16.	Plastic Deformation.....	34
Figure 6.1.	3D Strain Figure.....	41
Figure 6.2.	Strain ellipse.....	43
Figure 6.3.	Strain ellipse.....	44
Figure 6.4.	Shear strain parameters.....	45
Figure 7.1.	Triangles of the field.....	46

Figure 7.2.	Extensions and compressions accepted as homogeneous region.....	48
Figure 7.3.	The compression at the AVCT , KART and BOZT triangle .....	49
Figure 7.4.	Extensions at the MER1-AVCT-KART triangle .....	49
Figure 7.5.	Extensions BOZT-AVCT-BAD1 triangle .....	50
Figure 7.6.	Compression at the KART-BOZT-ULUT triangle.....	50
Figure 7.7.	Extension at the KART-MER1-MADT triangle.....	51
Figure 7.8.	Extensions and compressions for whole region accepted as homogeneous..	51
Figure 7.9.	Point P and its surrounding points .....	53

## LIST OF TABLES

Table 3.1.	Horizontal GPS velocities of the Marmara Region fixed to Eurasia.....	21
Table 5.1.	Strain parameters that are defined by repeated geodetic observations.....	36
Table 7.1.	Strain fields.....	45
Table 7.2.a.	Strain Tensor Parameters from Triangulation.....	46
Table 7.2.b.	Strain Tensor Parameters from Triangulation.....	46
Table 7.3.	Calculated Strain Parameters.....	48
Table 7.4.	Coordinate differences for infinitesimal homogeneous model .....	55
Table 7.5.	Infinitesimal strain parameters.....	57

## ACKNOWLEDGEMENTS

I would like to thank to my advisor Dr. Onur YILMAZ for guiding me during the thesis. His assurance, patience and valuables persistence makes me not to give up during my worse periods.

I would like to thank to Assoc. Prof. Dr. Haluk Özener for his support, encouragement, and guidance during my studies.

I could not have done my dissertation research without the help that I got from Assist. Prof. Dr. D. Ugur SANLI. I have learnt alot from you, stress can cause panic, and panic cause mistakes in the academic life.

I could not have survived the last year without support of my family and friends. I would like to thank my mum, Kevser Limon for providing me very peaceful study area at home. I am very thankful to my friends who are always near me. Thanks to Gozde Akay, Ilke Deniz, Petek Tatli and Saygin Abdikan.

I also would like to thank to my fiance, Martin SØRENSEN for his incomparable support, motivation, and understandings during my stressful times.

## **ABSTRACT**

### **ANALYSIS OF STRAIN ACCUMULATION OF THE FAULTING ZONES BY THE HELP OF CONTINUOUS GPS STATIONS**

The North Anatolian Fault Zone (NAFZ) belongs to one of the largest recent active fault systems in the Earth and it is the most effective zone in the Anatolian Plate. During the last decades a westward expansion of large earthquakes along the North Anatolian Fault has extended till the Sea of Marmara. The researchers give attention to the seismic gap in the Marmara Sea. It is expected that northern and middle strand of NAFZ have a strong risk for future actions.

The purpose of this study has two main goals. First one is to estimate velocity field of the region, and the second one is to investigate changes of the strain accumulation in the region by seven continuous GPS stations. This investigation is done by triangulation method and by using GPS coordinate differences obtained from 2002 to 2004 periods. Strain parameters such as maximum and minimum principal strains, direction of the maximum and principal strain, maximum shear strain parameters and its direction are determined.

## ÖZET

### SABİT GPS İSTASYONLARI KULLANILARAK FAY KUŞAĞI GERİNİM BİRİKİMİNİN ANALİZİ

Kuzey Anadolu Fay Kuşağı Dünyanın en geniş aktif fay sistemleri arasında bulunmaktadır ve Anadolu Plakasının en etkili kuşağıdır. Son yıllarda Kuzey Anadolu Fay Kuşağı boyunca batı yönündeki genişlemeler Marmara Denizine kadar ulaşmaktadır. Araştırmacılar Marmara Denizi içerisindeki sismik boşluğa dikkat çekmektedirler. Çünkü bu boşluk KAFZ' un kuzey ve orta bölgelerinde gelecek için büyük bir risk taşımaktadır.

Bu çalışmanın iki amacı vardır. Birincisi bölgedeki hız alanının belirlenmesi ve ikincisi ise yedi sabit GPS istasyonundan alınan verilerle gerinim analizinin hesaplanmasıdır. Bu araştırma üçgenleme ve koordinat farkları alınarak yapılmıştır. Gerinim parametreleri; maksimum minimum asal gerilme, maksimum-minimum gerinim parametrelili dönüklüğü, maksimum kayma gerinimi olarak tanımlanmıştır.

## TABLE OF CONTENTS

ACKNOWLEDGEMENTS.....	iii
ABSTRACT.....	iv
ÖZET.....	v
LIST OF FIGURES.....	viii
LIST OF TABLES.....	xi
1. INTRODUCTION.....	1
2. GENERAL TECTONIC OF NORTH ANATOLIAN FAULT ZONE (NAFZ) AND MARMARA REGION.....	3
2.1. North Anatolian Fault (NAFZ).....	3
2.2. Tectonics of Marmara Region.....	6
2.3. Seismicity in the Marmara Region.....	9
3. GPS DATA ANALYSIS.....	12
3.1. GIPSY Software.....	13
3.2. Data Analysis With GIPSY.....	14
3.3. Precise Point Positioning (PPP).....	18
3.4. Evaluation of Velocity Field.....	19
4. BASICS OF STRESS AND STRAIN.....	23
4.1. Stress.....	23
4.2. Strain.....	24
4.2.1. Two Dimensional (2D) Strain.....	24
4.2.2. Measuring Deformation.....	26
4.2.2.1. Length Deformation.....	28
4.2.2.2. Volume Deformation (Dilation).....	29
4.2.2.3. Rotational Deformation.....	30
4.3. Relationship between stress and strain.....	33
5. STRAIN ANALYSIS WITH GEODETIC METHODS.....	35
5.1. Methods and horizontal strain rate distribution.....	36
5.1.1. Discrete triangle method.....	37
5.1.2. Coordinate Differences.....	39

6. STRAIN ANALYSIS.....	40
6.1. Strain Tensor.....	40
6.2. Strain Elipse.....	43
7. DETERMINATION OF STRAIN FIELD IN THE WESTERN PART OF NORTH ANATOLIAN FAULT ZONE.....	45
7.1. Computation of Strain Parameters with Triangulation.....	45
7.2. Computation of Strain Parameters with Infinitesimal Strain Method.....	53
8. CONCLUSION.....	58
REFERENCES.....	60

## 1. INTRODUCTION

Global Positioning System (GPS) has been a very useful tool for the last two decades in the area of geodynamics. Its high accuracy in determination of relative positioning availability together with its modest budget increase the use of GPS all around the world.

GPS measurements are used to determine the strain accumulation along fault lines. Moreover, GPS measurements provide a significant tool for determining tectonic strain rates, which are assumed to be indicative of earthquake potential (Jackson, D.D et al., 1999). GPS measurements can be analyzed in two main method as continuous and campaign measurements.

The Marmara Continuous GPS network (MAGNET) was established to measure the deformations associated with strain accumulation along the western NAF system. After the 1999-earthquakes the network was extended to track the postseismic deformations caused by the earthquakes and to monitor the different fault systems in the Marmara region (Reilinger et al., 2000; Bürgmann et al., 2002a, 2002b; Hearn et al., 2002; Ergintav et al., 2002). It consists of 18 sites (Figure 1.1.).

In this study, strain accumulation around the fault zones at western Marmara was calculated. Seven continuous GPS MAGNET stations of The Scientific and Research Council of Turkey (TUBITAK) were used in order to determine the accumulation. These points are AVCT (Avcilar), BAD1 (Buyukada), MADT (Marmara Adasi), MER1 (Marmara Ereglisi), KART(Karacabey), ULUT (Uludag) and BOZT (Bozburun).

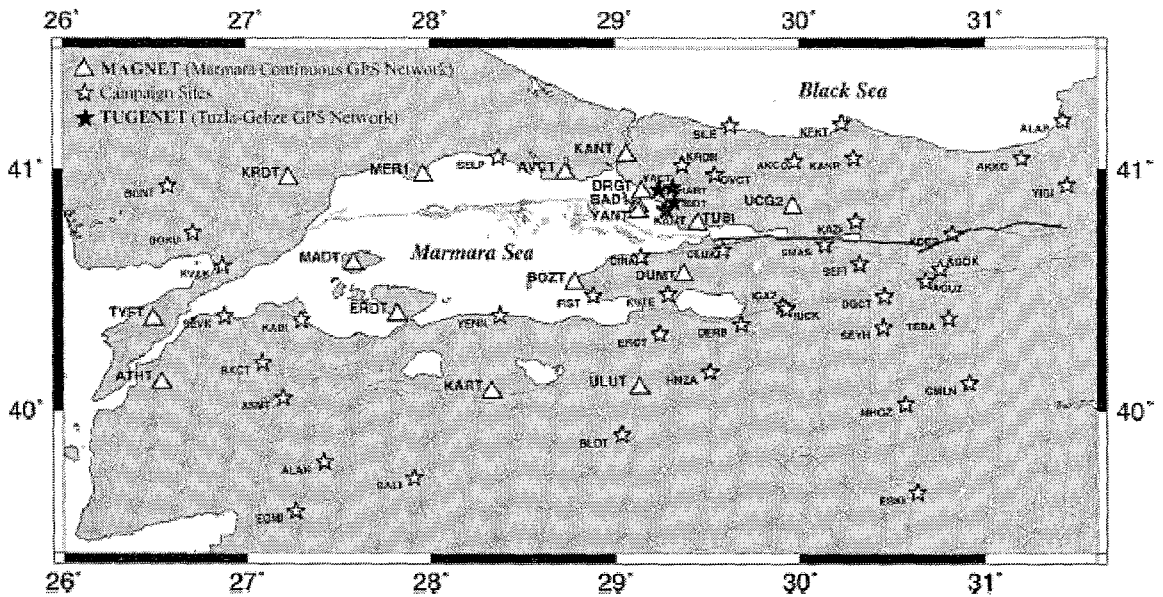


Figure 1.1. The distribution of continuous (MAGNET, TUGENET) and campaign GPS sites, adopted from TUBITAK.

The main goal of this study is first determine the velocities of the stations and then define the strain accumulation. For the determination of velocities, GIPSY software was used, and velocities were measured according to precise point positioning which is included in GIPSY. The results were compared to Ergintav et al. research and the similarities and differences between two study was explained.

Two different method are used for strain accumulation. These are triangulation and infinitesimal homogeneous model methods. Triangulation was done for six separate region and infinitesimal method was applied for every point.

According to the these methods the strain parameters were calculated and explained at the conclusion part. An example for each method can be seen at seventh part. Since the computation consists matrix calculation, MATLAB 7.0 software was used for matrix calculations.

## 2. GENERAL TECTONIC OF NORTH ANATOLIAN FAULT ZONE (NAFZ) and MARMARA REGION

### 2.1. North Anatolian Fault (NAFZ)

The Anatolian block is a small continental plate that is between the Arabian Plate, African plate and the Eurasian plate. The African Plate is moving counterclockwise and the Arabian Plate is moving northward into the southern side of the Eurasian Plate. The movement of these other plates forces the smaller Anatolian Block to move towards the west and southwest. The block is rotating counterclockwise as it escapes westwards from the collision zone between the Eurasian and Arabian plates (Figure 2.1.).

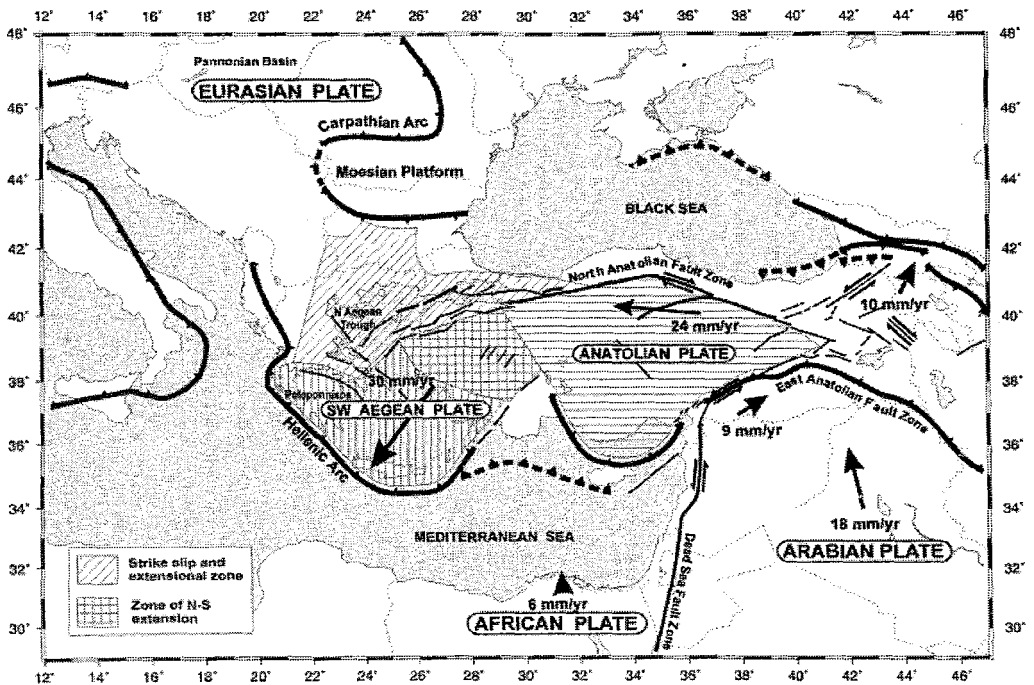


Figure 2.1. Simplified tectonic map of the Eastern Mediterranean with zones of coherent motion (McClusky et al., 2000).

The North Anatolian Fault (NAF) is one of the most important active continental strike slip fault systems in the world. It is also the most important fault zone in Turkey that produces lots of earthquakes that cause deaths, wounds and loss of property in large scale such as 9 August 1912 Saros-Marmara:  $M_s=7.4$ , 18 June 1953 Edirne:  $M_s=5.2$ , 18 September 1963 Yalova-Cinarcik:  $M_s=6.4$ , 6 October 1964 Manyas:  $M \sim 6.9$ , 23 August 1965 Saros:  $M_s=5.9$ , 22 July 1967 Mudurnu-Adapazari:  $M_s=7.1$ , 27 March 1975 Saros:  $M_s=6.6$ , 17 August- 12 November 1999 Golcuk and Duzce.

North Anatolian Fault Zone starts from Eastern Anatolia, Karliova, and runs parallel to the coast of Black Sea, and continues through the Aegean Sea over a length of more than 1500 km. The North Anatolian Fault (NAF) has almost entirely ruptured during a series of large earthquakes in the past century. The sequence propagated 800km westward between 1939 and 1999; and 12 major earthquakes ( $M>6.7$ ) occurred and ruptured NAFZ (Figure 2.2.). Those westward-direction displacements have a cumulative value of over 1000 km. This is thought to occur as each earthquake transfers its stress to another region along the fault zone.

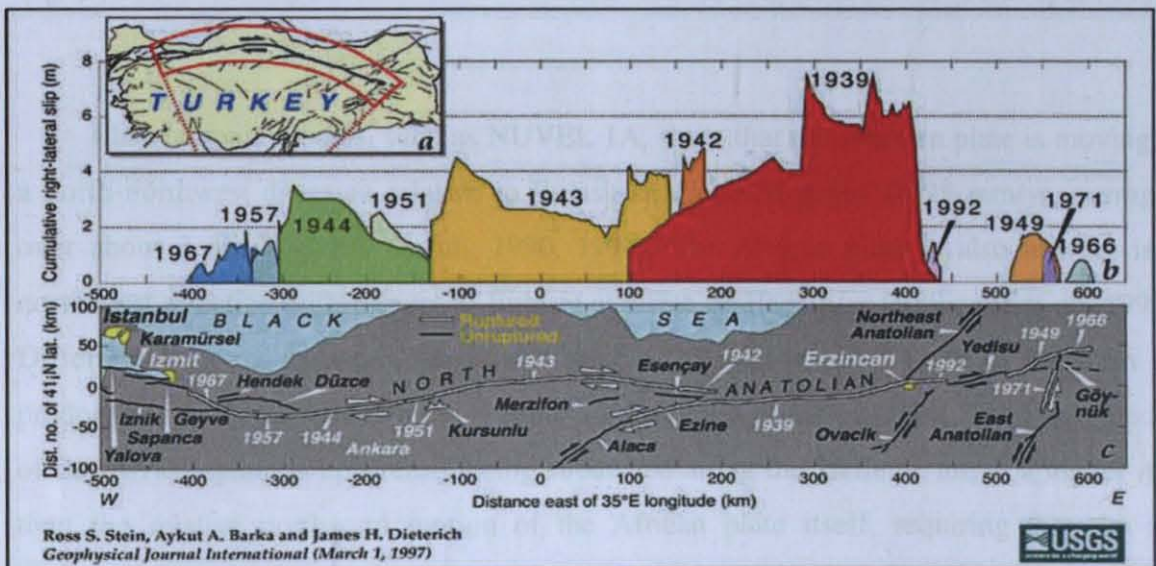


Figure 2.2. Surface ruptures and cumulative slips along NAFZ. (Stein et.al., 1997)

North Anatolian fault has many characteristics similar to California's San Andreas fault (Figure 2.3.). These two faults are right-lateral, strike-slip faults having similar lengths and similar long-term rates of movement. If a person is looking across a right-lateral, strike-slip fault during such an earthquake, that person would see the opposite side move to the right.

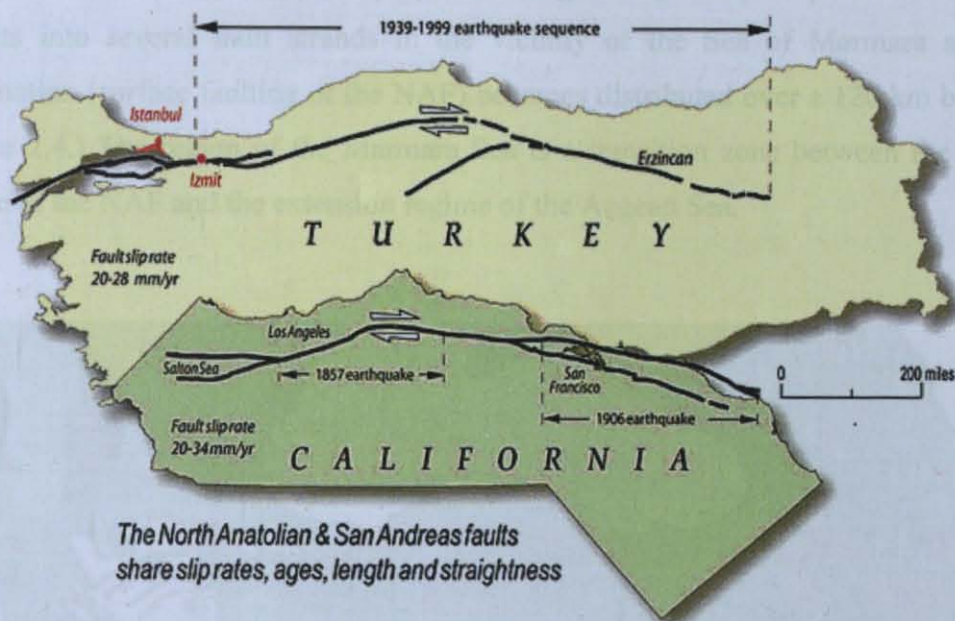


Figure 2.3. Similarity between North Anatolian and San Andreas Faults (Stein et al., 1999)

Plate tectonic models, such as NUVEL 1A, show that the Arabian plate is moving in a north-northwest direction relative to Eurasia at a rate of about 18-25 mm/yr, averaged over about 3 Ma (DeMets et al., 1990, 1994). The African plate is also moving in a northward direction with respect to Eurasia at a rate of 10 mm/yr (Reilinger et al., 1997). Differential motion between Africa and Arabia (15 mm/yr) is thought to be taken up predominantly by left-lateral motion along the Dead Sea transform fault. The leading edge of the African plate is apparently being subducted along the Hellenic arc at a higher rate than the relative northward motion of the African plate itself, requiring that the arc (presumably the Aegean Sea) moves southward relative to Eurasia proper (Oral et al., 1995).

## 2.2. Tectonics of Marmara Region

The Sea of Marmara is a marine basin in northwest Turkey that connects the Aegean Sea with the Black Sea, and includes a series of tectonically active basins at the western end of the right-lateral North Anatolian Fault (NAF) (Sengor et al. 2002). Across most of Turkey the NAF is a relatively simple, narrow, right-lateral strike-slip fault zone; however it splits into several fault strands in the vicinity of the Sea of Marmara so that the deformation (surface faulting of the NAF) becomes distributed over a 120 km broad zone. (Figure 2.4.) The region of the Marmara Sea is a transition zone between the strike slip regime of the NAF and the extension regime of the Aegean Sea.

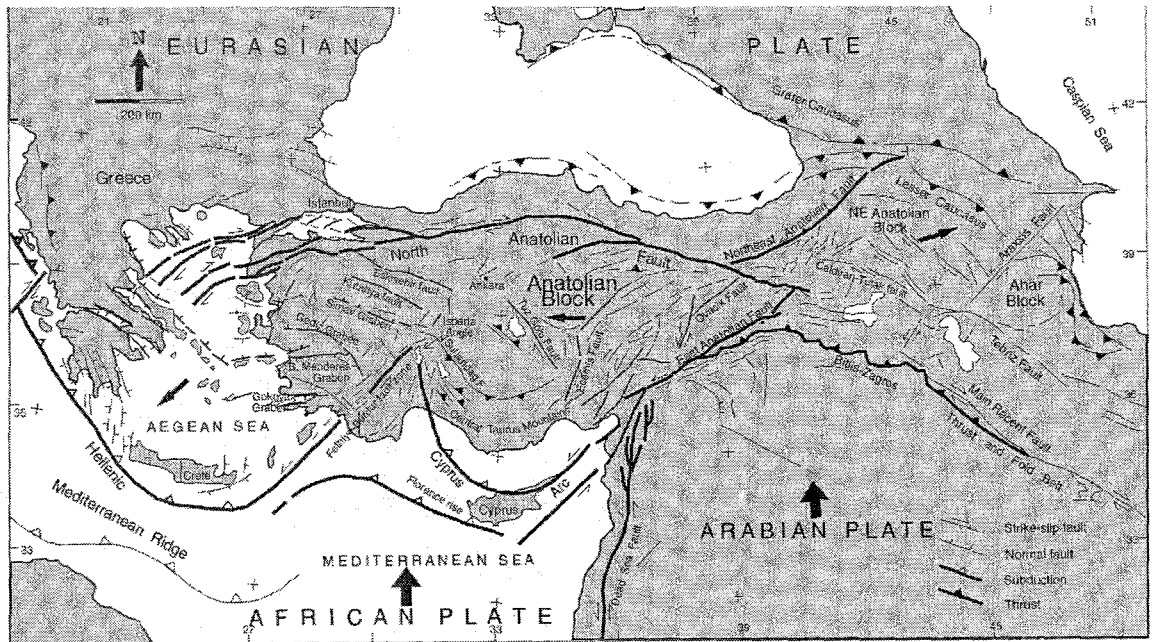


Figure 2.4. Distribution of active faults in the Anatolian region. (Barka et al., 1997).

The tectonics of the Marmara region were studied by many earth scientists (Ketin 1973, Ucer et al. 1997, Barka 1997). There are still some topics to be clarified due to the very complex structure of the region, although many aspects were clarified. Barka summarised these works at 1997. According to Barka, many tectonic events are related with the North Anatolian Fault. This fault splits into three strands in the vicinity of

Mudurnu valley. These strands are named as northern, central and southern strands. The northern strand passes through the Izmit bay, Marmara through and Saros gulf and extends towards Greece. The central strand follows the path through Geyve, Iznik, Mudanya, Bandirma and Biga. The southern strand follows the path through Bursa, Manyas Lake, Balikesir and Edremit Gulf. In addition to them, in his extensive work, Barka also summarised that; the basins in the Marmara Sea and Lakes of Sapanca, Iznik and Manyas are considered to be as a result of pull-apart mechanism associated with the strike-slip motion of the strands of NAF (Figure 2.5.).

Furthermore, in addition to strands of the NAF, the tectonics of the Marmara region are also influenced by Istranca fault, Terzili fault in Trakya (Thrace) which may be the continuations of some faults originating in the Anatolian Plate and extending into Trakya (Barka et al, 1997).

The main branch of the dextral strike-slip North Anatolian fault enters to Marmara Sea through the Gulf of Izmit to the east and comes out through the Ganos fault, north of the Gallipoli peninsula, to the west.

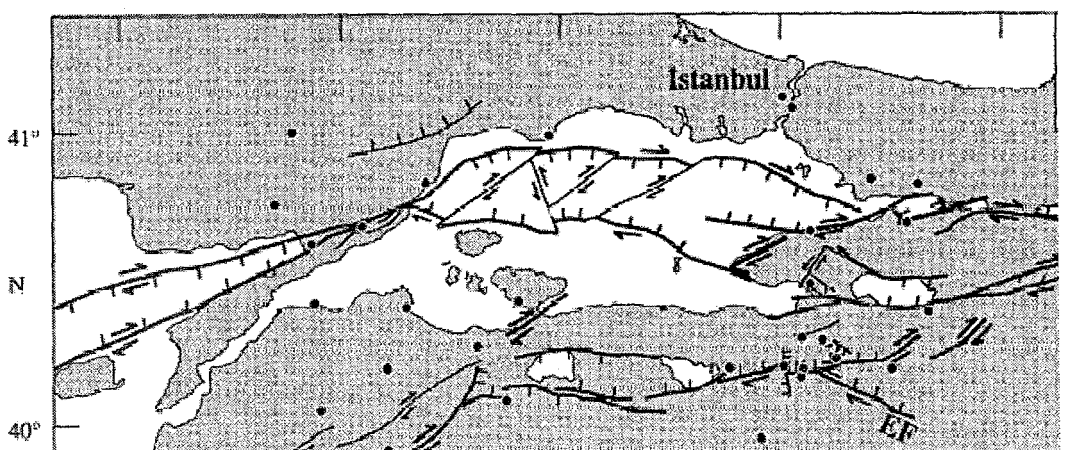


Figure 2.5. The Marmara region showing the mapped faults (Barka&Kadinsky-Cade 1988; Saroglu et al., 1992. Armijo et al., 2002)

An updated version of the velocity field reported by McClusky *et al.* (2000) highlights the main tectonic elements of the region (Figure 2.6.). Velocity vectors in the south are dominated by large (~25 mm/yr) westward components and show the relative motion of Turkey with respect to Eurasia (McKenzie, 1972). The magnitude of the velocity vectors decreases rather regularly with latitude.

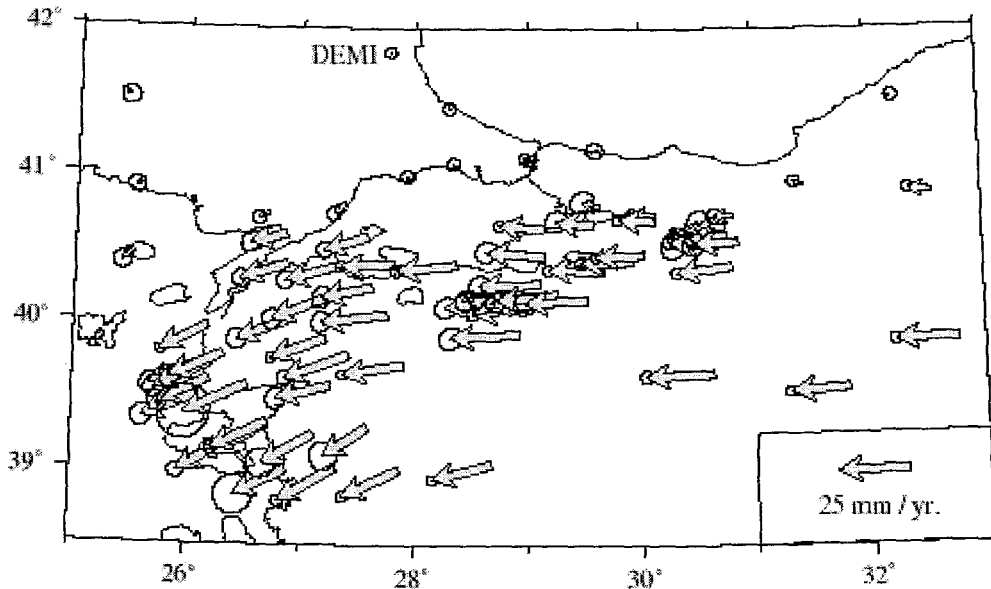


Figure 2.6. Updated GPS velocities near the Marmara Sea region, after McClusky *et al.* (2000).

Closer to the Marmara Sea significant differences occur. It is easier to understand the whole region when vectors are referenced to Eurasia. The significance of vectors in the immediate Marmara region is clearer when referenced to Anatolia (Figure 2.7.). In this figure it can be seen that many vectors are orientated approximately perpendicular to the overall direction of motion on the boundary.

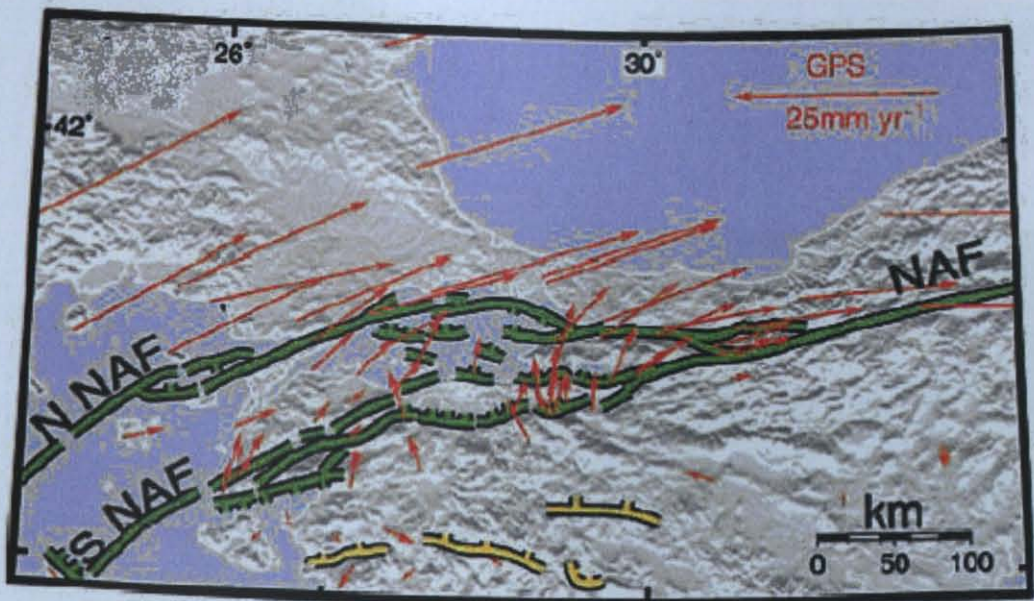


Figure 2.7. Mapped faults and GPS vectors referenced to fixed Anatolia (obtained by removing the Anatolia/Eurasia rotation of McClusky et al. 2000)

### 2.3. Seismicity in the Marmara Region

In the Marmara Sea region, historic seismic activity is prominent (Ambraseys & Finkel 1991); many devastating earthquakes have occurred along the NAFZ. The instrumentally covered period shows that in the last decades seismicity of Western Anatolia has been highly active character. Detailed investigations of low-magnitude earthquakes reveal swarm-type activity with remarkable clustering in space and time (Ücer et al. 1985, 1997, Sellami et al. 1997). The fault mechanisms of strong earthquakes are associated with major tectonic structures (Jackson & McKenzie 1988, Papazachos & Kiratzi 1996).

Seismicity of the Marmara region is relatively very high as indicated by both the historical and recent (instrumental period) devastating earthquakes (Figure 2.8.). The high rate of seismicity has a critical importance for the earthquake hazard in the Marmara

region, because approximately one to fourth of Turkey's population and most of industrial centers are included in this region.

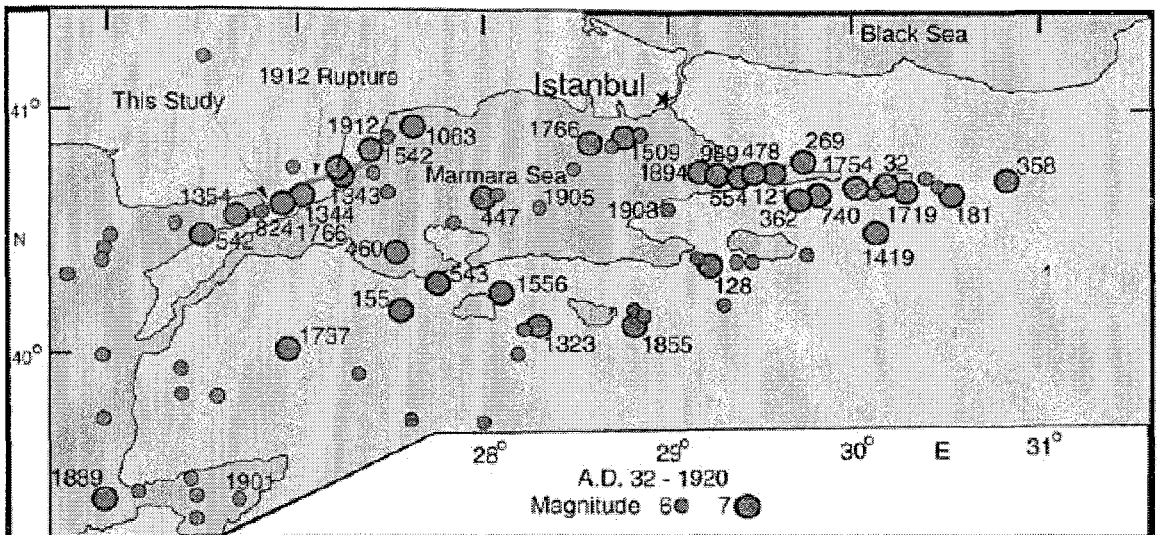


Figure 2.8. Historical seismicity of the Marmara Region; (Ucer et al., 1997)

The intensive scientific efforts are recently devoted to the Marmara Sea region because of the historical record of damage to large cities such as Istanbul, and the close proximity of the North Anatolian fault which is submerged beneath the Marmara Sea (McClusky et al., 2000).

The most recent probability estimate of a  $M \geq 7$  earthquake rupturing beneath the Sea of Marmara is  $\sim 35\text{--}70\%$  in the next 30 years if a time-dependent model that included coseismic and postseismic effects of the 1999  $M_w=7.4$  Gölcük-İzmit earthquake is used. This estimate of course incorporate recently obtained bathymetric images of the North Anatolian fault beneath the Sea of Marmara (Armijo et al., 2002) and improved earthquake catalog for the period between A.D. 1500 and 2000 using the regional attenuation relation of (Ambraseys, 2001).

In addition to the recent pattern of large earthquakes in western Turkey, longer-term studies of seismicity have suggested that the Marmara Sea region might be particularly susceptible to the occurrence of a large earthquake. Toksoz et al. (1979) concluded that an approximately 300-km-long segment of the fault system in the Marmara area has not ruptured seismically since the early sixteenth century and characterized the unbroken segment as a seismic gap capable of producing large earthquakes.

### 3. GPS DATA ANALYSIS

GPS is essential in applications that require high (sub centimeter) positioning precision, such as in the velocity field estimation of tectonic plates. Currently, GPS relative positioning or GPS Precise Point Positioning (PPP) used for such applications.

Nowadays, the monitoring of station coordinates located on the Earth's surface is of enormous interest. Determination of velocity fields provides a means of analysing inter- and intra-plate geodynamic interactions and other types of crustal disturbances.

The basic GPS observables used for estimating position, velocity and time are: Pseudo range and carrier phase or difference of carrier phase. Dual frequency data is required since ionosphere related errors can be eliminated by using data combinations based on two different frequencies.

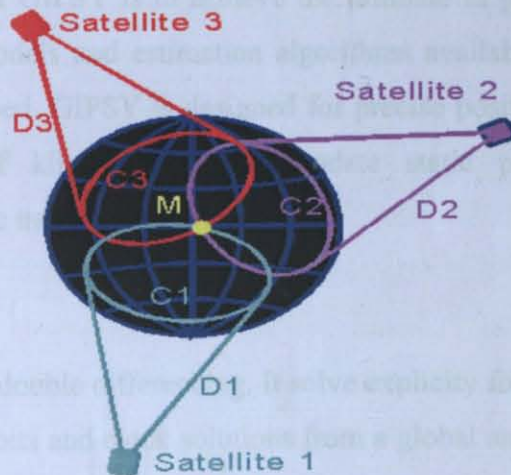


Figure 3.1. The geometric problem of 3-D positioning from ranges.

Pseudorange multipath is mainly governed by the following factors:

- the location of the antenna: is a ground plane or choke ring available, are higher conducting obstacles nearby,
- the quality of the antenna: does the antenna have low sensitivity for low elevation signals,
- the quality of the receiver: do the tracking algorithms of the receiver channels poses multipath reduction techniques.

The differences between the pseudo-range data and the carrier phase data are: (a) the ambiguity terms, (b) the reversal in the sign for the ionospheric delay, and (c) the significantly larger noise term associated with pseudo-range data. The multipath terms are not included, however, the pseudo-range data is more sensitive to multipath (hence a larger magnitude term) than carrier phase data.

### **3.1. GIPSY Software**

The primary goal of GIPSY is to achieve the ultimate in positioning accuracy. For that purpose, the best models and estimation algorithms available are incorporated, and new methods are developed. GIPSY is designed for precise positioning over distances of meters to thousands of kilometers. Accommodate static positioning, rapid static positioning, and kinematic tracking receivers.

GIPSY does not do double differencing. It solve explicitly for the satellite clocks, it is possible to use precise orbits and clock solutions from a global analysis to point position a single station at a time. This provide decreasing of the computation time of GPS data and clocks are estimated stochastically using white noise estimation. In addition to these, GIPSY uses random walk model for tropospheric zenith delay and for the ionosphere model L1 and L2 combinations are used (Sanli;1999).

GIPSY estimates parameters by filtering and smoothing. Filtering is based on forward processing of the measurements in time, and accumulating the solution and generating smoothing coefficients at each time step.

Smoothing does backward processing of the accumulated solution over all of the timesteps (epochs) using smoothing coefficients to apply information in the terminal solution to the stochastic parameters (Hurst, 1998; Bierman, 1977).

Ambiguity resolution is not mandatory for GIPSY global analysis, however studies suggest that it improves the accuracy of the horizontal components for local and regional networks by a factor of about 1.5 to 2.

A GIPSY user has various options for the use of orbits. Orbits can either be integrated with appropriate models using navigation files (broadcast ephemerides), or precise orbits can be hold fixed from IGS or JPL ftp sites (i.e. SP3 format for IGS and \*.eci, \*.shad, \*tpeo.nml format for JPL).

### **3.2. Data Analysis with GIPSY**

GIPSY consists of various individual processing modules (programs) written in Fortran or recently in C. They can be operated from the UNIX command line with a list of parameters and files as input. Every module creates output file(s) , which is input for the next module. Different modules can be arranged as batch processing to produce results according to a specific purpose. Unix shells are usually used to create such batch processing utilities, especially c-shell scripting. Figure 3.2 shows the flow chart of a typical GIPSY processing. In general, data analysis can be performed in five steps (Sanli, 1999):

1. Preparing (i.e. cleaning and compressing for the solution) data
2. Forming the design matrix,

3. Running solutions,
4. Applying filtering and least square (LS) estimation,
5. Removing outliers and reprocessing.

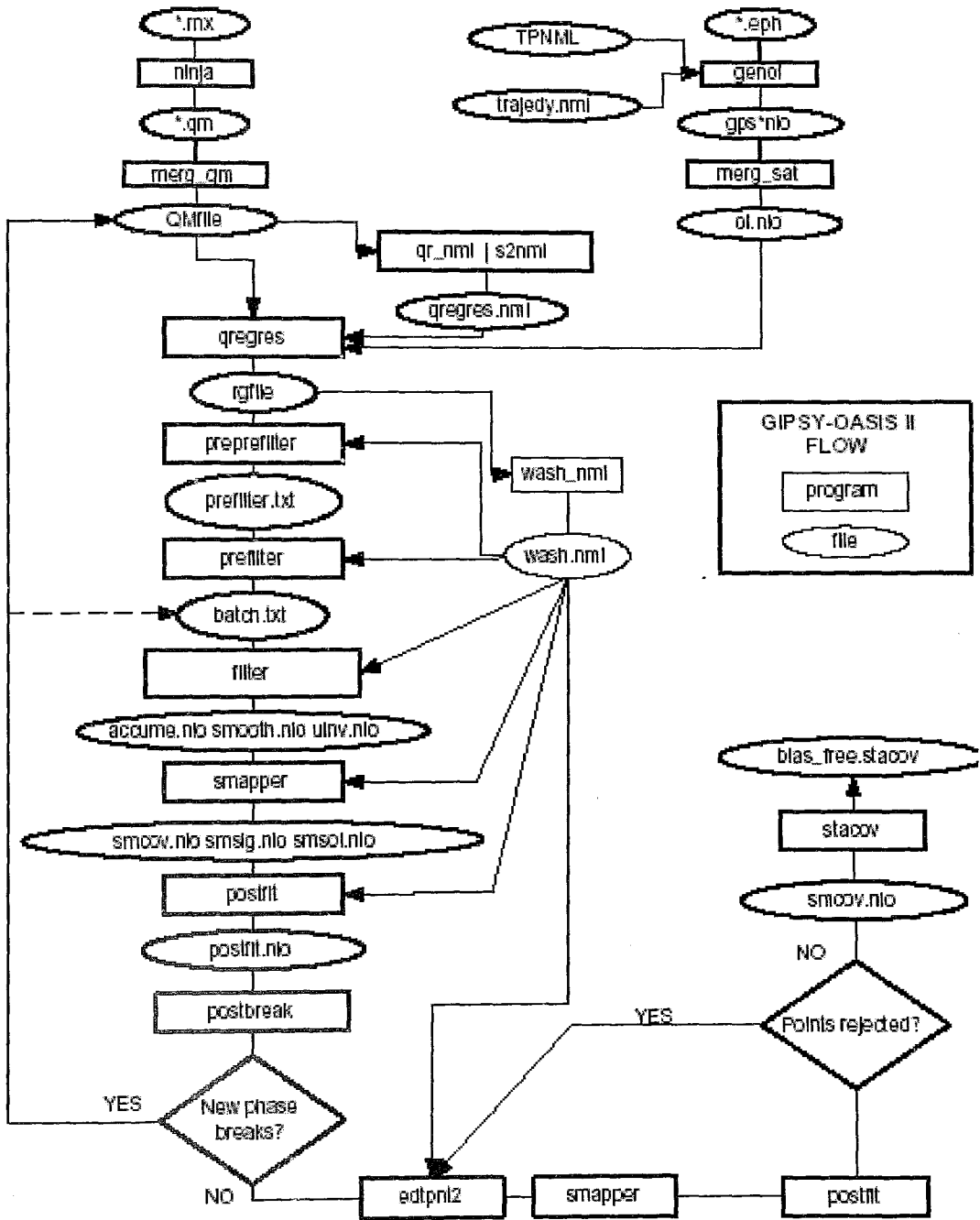


Figure 3.2. Flow chart of GIPSY process

In this study, geodetic positions of GPS benchmarks have been determined by GIPSY Precise Point Positioning. The brief description of GIPSY modes are defined below and also binary input and output files produced by the individual modules can briefly be followed from the flow chart of GIPSY (Figure 3.2).

### **Data Input and Editing (*ninja*, *merge\_qm*, *weed\_qm*):**

*Ninja* is always run for every file. It reads RINEX files, decimates the data to a user\_specified time interval and produces qm files. It can edit data automatically using the TurboEdit algorithm.

*Merg\_qm* merges multiple qm files into a single file. It is used to merge all qm files for a given day into a single file which represents all the data. This file is then used as the input to *qregres*.

### **Functional (Measurement and Earth) Model (*qr\_nml*, *qregres*):**

*Qregres* reads a merged qm file and computes a priori model and the partial derivatives required for the model matrix. Because the model for the GPS observables is not linear, the model is linearized about a priori values of station coordinates, satellite orbits, and other parameters (most other parameters have a priori values of zero). The prefit residuals and partial derivatives are stored in a regression file.

### **Parameter Estimation (*preprefilter*, *prefilter*, *filter*):**

*Preprefilter* reads part of the filter input file and prepares the input file for *prefilter*.

*Prefilter* prepares the batch file that tells the filter when each stochastic update will occur. Stochastic updates are used to estimate time-varying parameters such as clock offsets, tropospheric delays and phase ambiguities.

*Filter* is the estimation program. It is square root information factorized Kalman filter. It has capability to estimate time-varying (stochastic) parameters as well as standart constant parameters.

### **Smoothing and Computation of Covariances (smapper):**

*Smapper* is backward (smoother) step of the Kalman filter. This step is required in order to obtain estimates of time-varying parameters which are based on all of the data. Such estimates are required to compute the postfit residuals, for instance. *Smapper* is able to run quickly because all of the required matrices are stored in the files made by *filter*.

*Smapper* sends its output to the two important output files. One of them stores the final solution and covariance and the other one stores the estimates of each data epoch. The first one is read by *stacov*, or by any other program that needs to extract the solution. The second file is used by *postfit* to compute the post-fit residuals.

### **Computation of Residuals (postfit):**

*Postfit* computes postfit residuals. Besides this, it applies a test to each residual. Any residual larger than a user-specified tolerance is flagged as an outlier. This information is written out in a point file, which contains instructions needed to delete these points from solution. *Postfit* includes a log file that gives information about each "outlier" point.

### **Cycle Slip Detection (postbreak):**

*postbreak* detects the cycle slips missed through *ninja* by checking the discontinuities in post-fit residuals. If cycle slips are detected then *qm* file needs to be modified. Therefore processing has to be repeated starting with *gregres* (Figure 3.2). The procedure continues till cycle slips are completely fixed.

**Extracting Final Solution (stacov, statistics):**

*Stacov* is a program to extract the coordinates and covariance from a smoothed covariance file and save it in a smaller and more convenient form. It creates stacov files, which are easy to read ASCII files. The stacov file is then the input to the various postprocessing utilities.

*Statistics* computes coordinates, baseline components, and their repeatabilities in various coordinate systems.

**3.3. Precise Point Positioning (PPP)**

Precise Point Positioning (PPP), together with relative positioning, provides a significant contribution to geodynamic applications. One of the advantages of PPP is that positions are independently derived. Whereas in relative positioning, an error in the base station coordinates would translate into the other stations. In PPP, dual-frequency data is essential. Therefore, there are two observation equations, for both pseudo range and carrier phase. PPP analysis of GPS data is described in Zumberge et al. (1997).

The software used for the processing of the GPS data is GIPSY OASIS II (GPS Inferred Positioning SYstem Orbit Analysis and Simulation Software), (Gregorious, 1996). It is capable of PPP processing of the GPS data as well as processing of SAR and DORIS data. In this study seven continuous GPS points of Marmara GPS Network (MAGNET) were used. These points are located at the the Marmara region. Figure 3.3 shows the locations of the seven GPS points used in the processing. Data was collected over a period of three years, between 2002 and 2004.

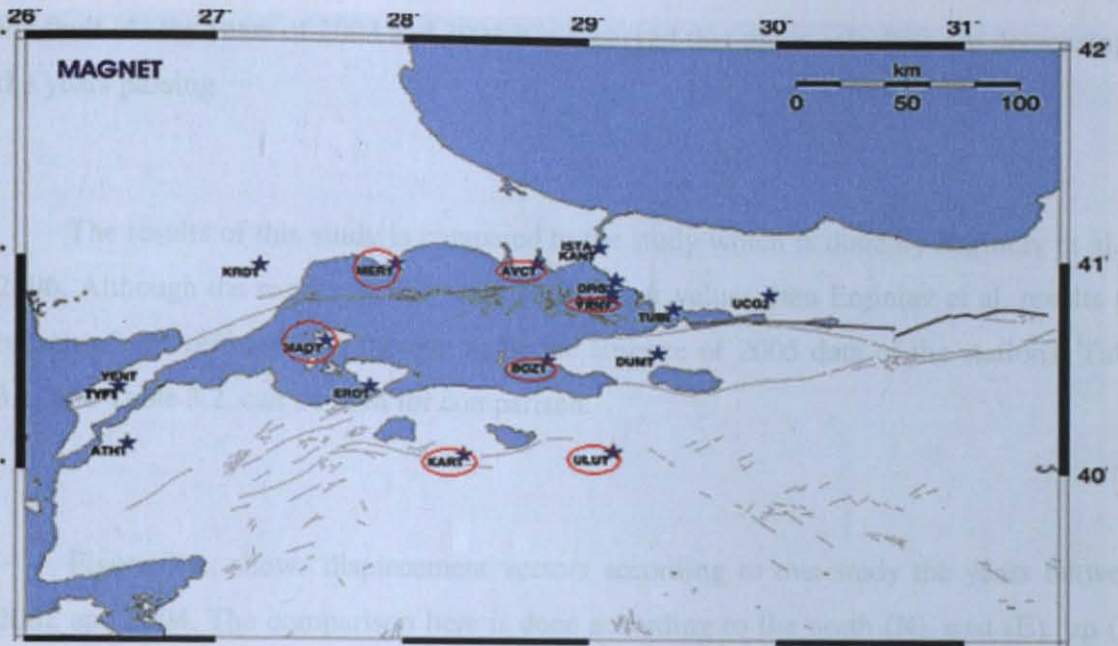


Figure 3.3. GPS Points used in this study. (Taken from TUBITAK MAM)

### 3.4. Evaluation of Velocity Field

The observation of transient postseismic ground deformations following major earthquakes is an important tool to understand the mechanics of the earthquake process and the mechanical behavior of the region surrounding the fault zone. Transient postseismic deformations can continue from immediately after the earthquake time to several tens of years as a function of time dependent stress relaxation (Ergintav et al., 2002).

Marmara Region, provide the opportunity to improve significantly the understanding of the mechanical behavior of the western part of North Anatolian Fault.

Figure 3.4. Displacements of stations between 2002 and 2004

In this study, the results of GIPSY Software shows that at the year of 2002, the velocities of stations close to fault are two times as big as the ones which are far away from

the fault. At the years of 2003 and 2004 it is observed that these velocities are decreasing y the years passing.

The results of this study is compared to the study which is done by Ergintav et al. at 2006. Although the results of this study have bigger values than Ergintav et al. results the reason of this difference is thought to be the absence of 2005 data of the stations. Table 3.1. and Table 3.2. can be seen for comparison.

Figure 3.4., shows displacement vectors according to this study the years between 2002 and 2004. The comparison here is done according to the north (N), east (E), up (U) values. Although the concept of N, E, U values are different from latitude and longitude values, when the results are converted to each other it can be seen that there is no significant difference. The negative values of velocities show the motion at opposite direction.



Figure 3.4. Displacements of stations between 2002 and 2004

Table 3.1. Horizontal GPS velocities of the Marmara Region at Eurasian fixed frame  
(S. Ergintav et al., 2006)

Site	Longitude ( $\theta$ )	Latitude ( $\theta$ )	E&N rate (mm/year)		E&N (mm/year) $\pm$	
ULUT	29,131	40,098	-23,02	-2,59	0,30	0,28
BAD1	29,118	40,852	0,29	1,20	0,31	0,29
BOZT	28,782	40,534	-15,84	-2,82	0,46	0,48
AVCT	28,724	40,989	-4,84	3,11	0,41	0,42
KART	28,333	40,265	-19,69	-2,11	0,28	0,26
MER1	27,962	40,967	1,10	1,87	0,29	0,26
MADT	27,587	40,611	-15,86	-3,30	0,37	0,38

Table 3.2. Velocity of stations according to this study

STATION ID	YEAR	LATITUDE (°)	LONGITUDE (°)	VELOCITIES		E&N	
				LAT (mm/y)	LON (mm/y)	(mm/year) ±	
AVCT	2002	40,9886662	28,7238594	2,56	37,32	2,32	4,31
AVCT	2003	40,9886664	28,7238599	18,55	14,03	1,87	3,25
AVCT	2004	40,9886665	28,7238600	34,56	15,4	2,82	5,32
BAD1	2002	40,8521167	29,1178962	-5,37	31,49	3,69	5,93
BAD1	2003	40,8521168	29,1178964	8,62	34,38	1,98	3,56
BAD1	2004	40,8521169	29,1178967	11,6	23,65	2,02	4,32
KART	2002	40,2652583	28,3325650	3,75	10,33	1,57	2,80
KART	2003	40,2652583	28,3325650	6,48	9,05	2,20	3,81
KART	2004	40,2652584	28,3325650	10,26	13,59	2,27	4,61
MADT	2002	40,6113518	27,5869420	-9,50	18,00	1,90	3,23
MADT	2003	40,6113518	27,5869419	4,62	12,13	1,70	2,83
MADT	2004	40,6113519	27,5869420	9,25	13,95	2,36	4,16
MER1	2002	40,9669334	27,9617481	4,19	35,13	3,12	5,44
MER1	2003	40,9669335	27,9617484	8,90	35,65	2,86	5,17
MER1	2004	40,9669336	27,9617488	15,88	38,02	4,98	14,63
ULUT	2002	40,0975482	29,1314441	3,44	9,01	1,43	2,20
ULUT	2003	40,0975483	29,1314441	7,24	9,63	1,72	3,06
ULUT	2004	40,0975483	29,1314441	6,64	8,42	2,26	3,97
BOZT	2002	40,5343851	28,7820346	-14,82	16,82	5,27	8,78
BOZT	2003	40,5338509	28,7820343	6,11	19,59	2,41	4,10
BOZT	2004	40,5343852	28,7820347	0,07	15,87	2,72	4,86

## 4. BASICS OF STRESS AND STRAIN

### 4.1. Stress

Stress is defined as force per unit area. It has the same units as pressure, and in fact pressure is one special variety of stress. However, stress is a much more complex quantity than pressure because it varies both with direction and with the surface it acts on. If stress is not equal from all directions then we say that the stress is a differential stress.

Three kinds of differential stress occur (Figure 4.1).

- Tensional stress (or extensional stress), which stretches rock;
- Compressional stress, which squeezes rock; and
- Shear stress, which result in slippage and translation.

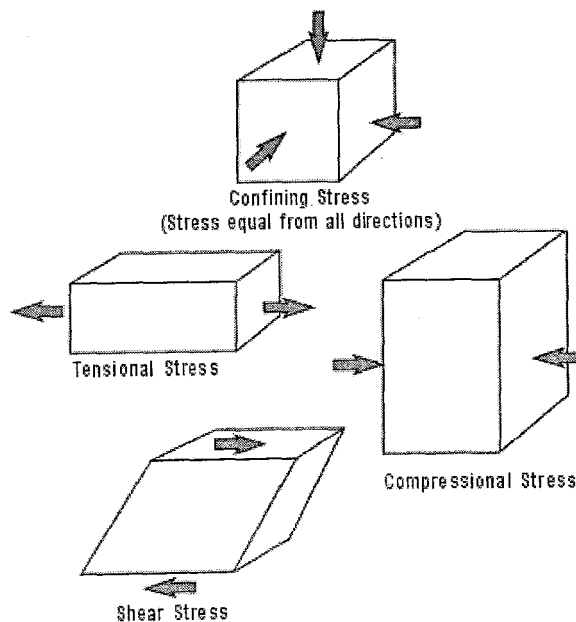


Figure 4.1. Three kinds of differential stress

Stress is not directly measurable, but nevertheless it is important to know the stress situation for reconstructing and estimating tectonic regimes, and for assessing fault kinematics. It is generally assumed that, in the plate-tectonic framework, large scale deformations occur due to local response of the lithosphere to induced stresses. Understanding the origine and distinguishing the different types of these stresses, as well as knowing their orientations and magnitudes is therefore a crucial tool in analysing and understanding tectonic deformation.

## 4.2. Strain

The motions of tectonic plates apply tremendous forces to the earth's crust. The forces change with changing plate configurations, leading to variations in states of stress in rocks. When forces, and thus stress are applied to rocks, the rocks may change position and shape. The change in position is known as displacement. The change in shape is known as strain. In general, strain is used for the determination of deformation.

### 4.2.1. Two Dimensional (2D) Strain

If the relative positions of the particles of a body are changed so that their initial and final positions can not be made to correspond by movement as a rigid body (translation, rotation) the body said to be strained. There are two strain types, homogeneous strain and inhomogeneous (heterogeneous) strain (Figure 4.2 and 4.3). This study was made according to the homogeneous strain measurements.

Homogeneous strain is defined by below geometrical criteria:

- straight lines remain straight after deformation,

- parallel lines remain parallel after deformation,
- all lines in the same directions in the strained body have constant values of shear strain and longitudinal strain,
- Circles become ellipses,
- 3-D spheres become ellipsoids.

Changes of lengths and angles are commonly used in analysis of strain.

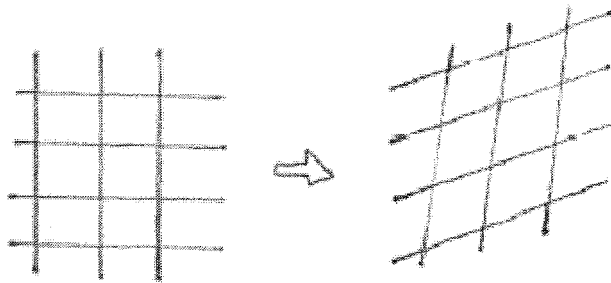


Figure 4.2. Homogeneous strain

For the heterogeneous strain; strain is different in various parts of the rock body. one or more of homogeneous strain conditions do not apply.

- Original straight lines do not remain straight,
- Original parallel lines do not remain parallel,
- Circles do not become ellipses,
- 3-D spheres do not become ellipsoids.

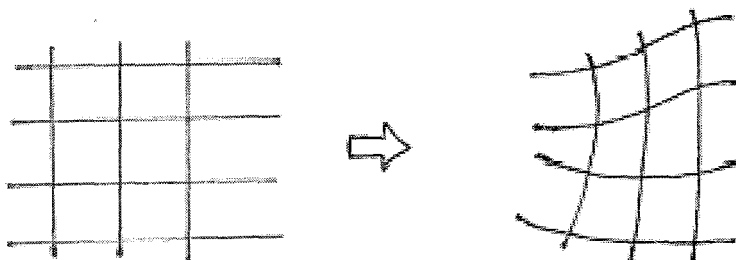


Figure 4.3. Heterogeneous strain

### 4.2.2. Measuring Deformation

The collective displacements of points in a body relative to an external reference frame is known as deformation. Deformation describes the transformations from some initial to some final geometry. Deformation of a rock body occurs in response to a force.

The response of a rock body to a force involves any one or a combination of four components divided into rigid and non-rigid body deformation. With rigid body deformation the position and orientation of points in a rock body relative to an internal reference frame are not changed. Rotation is a rigid body operation that changes the configuration of points relative to some external reference frame in a way best described by rotation about some axis (Figure 4.4.). Translation is another variety of rigid body deformation, which involves a change in position.

During pure translation, a body of rock is displaced in such a way that all points within a body move along parallel paths relative to some external reference frame (Figure 4.5.). Non-rigid body deformation is different than rigid body deformation in that the position and orientation of points within a rock body are changed relative to both an internal and external reference frame.

Distortion is a non-rigid body operation that involves the change in the spacing of points within a body of rock in such a way that the overall shape of the body is altered with or without a change in volume (Figure 4.6.). Dilation is a non-rigid body operation involving a change in volume. When pure dilation takes place without a change in shape, internal points of reference spread apart or pack closer together in such a way that line lengths between points become uniformly longer or shorter and the overall shape remains the same.

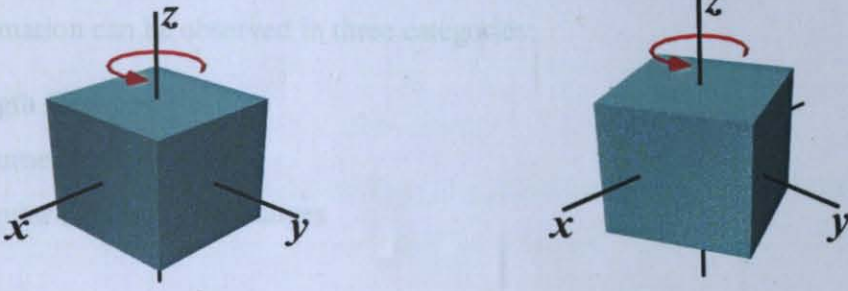


Figure 4.4. The blue cube is rotated in a clockwise direction about the  $z$ -axis.

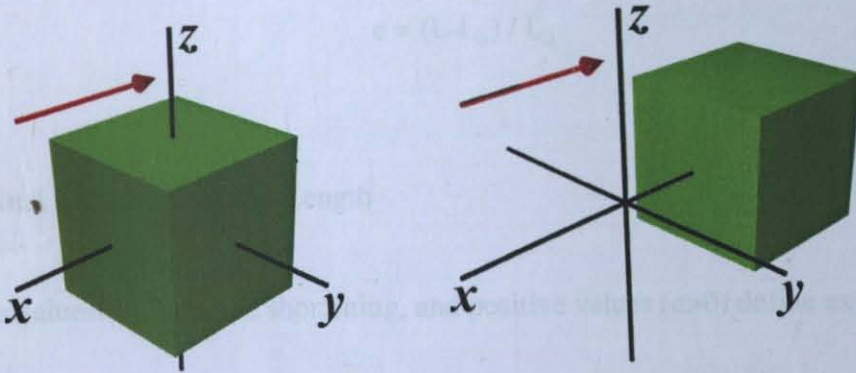


Figure 4.5. The green cube is translated parallel to the  $x$ -axis.

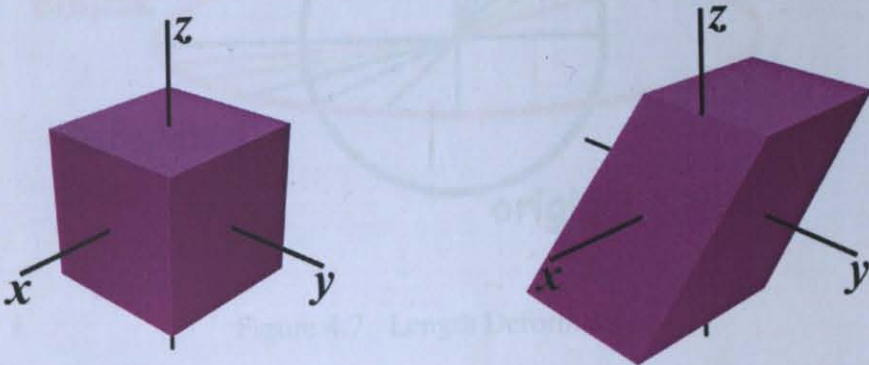


Figure 4.6. The purple cube is being distorted or strained.

Deformation can be observed in three categories:

1. Length Changes
2. Volume Changes
3. Angular (Rotational) Changes

**4.2.2.1. Length Deformation.** a) The longitudinal strain,  $e$ , is measured in terms of the changes in distance between two points (Figure 4.7).  $e$  (Extension) is a dimensionless quantity.

$$e = (L - L_0) / L_0 \quad (4.1)$$

$L_0$  = Original Length ;  $L$  = Final Length

Negative values ( $e < 0$ ) define shortening, and positive values ( $e > 0$ ) define extension.

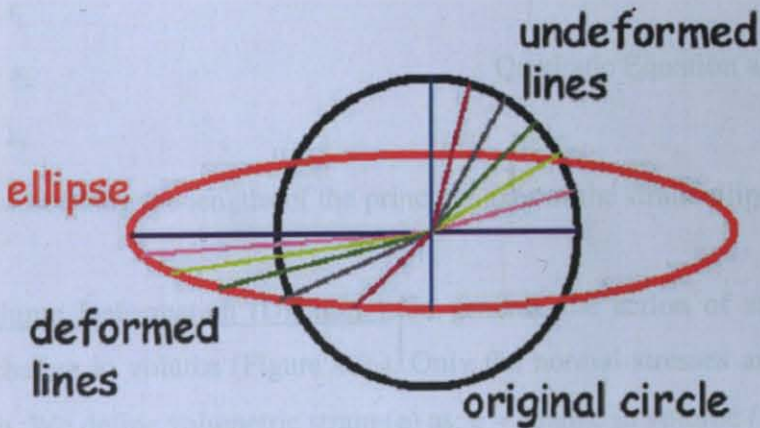


Figure 4.7. Length Deformation

As it is seen on the above figure; magenta line is shortened and pink line is lengthened during the deformation.

b) Quadratic Elongation ( $\lambda$ ) is an alternative expression for length changes.

$$l = s^2 = (1+e)^2 \quad (4.2)$$

c) Stretch ( $s$ ) is the ratio of the line's deformed length to the undeformed length. These principal stretches represent the semi-length of the principal axes of the strain ellipsoid. (Figure 4.8.)

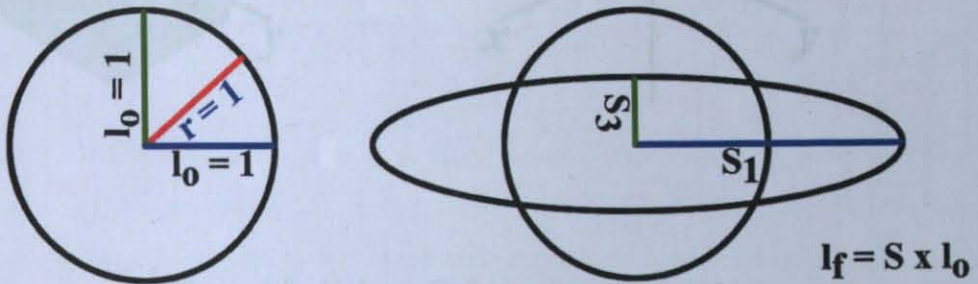


Figure 4.8. Stretch figure

$$\text{Stretch: } s = l/l_0 = 1+e = \lambda^{1/2} \quad (\text{no dimension}) \quad (4.3)$$

$$x = \sqrt{(\lambda_1)} = s_1$$

$$y = \sqrt{(\lambda_2)} = s_2$$

$$z = \sqrt{(\lambda_3)} = s_3$$

$$\text{Quadratic Equation and Stretch} \quad (4.4)$$

are useful in describing the lengths of the principal axes of the strain ellipsoid.

4.2.2.2. Volume Deformation (Dilation): In general, the action of stresses will cause material to change in volume (Figure 4.9.). Only the normal stresses are associated with volume strain. We define volumetric strain ( $e$ ) as:  $e = \text{change in volume} / \text{original volume}$

Volumetric Strain ( $\Delta$ ), Volume Change (dilation);

$$(\Delta) = (V - V_0) / V_0 \quad (4.5)$$

$V_0 = \text{Original Volume,}$   $V = \text{Final Volume.}$

$\Delta$  is a dimensionless quantity. Negative values show decreasing volume, and positive values show increasing volume.

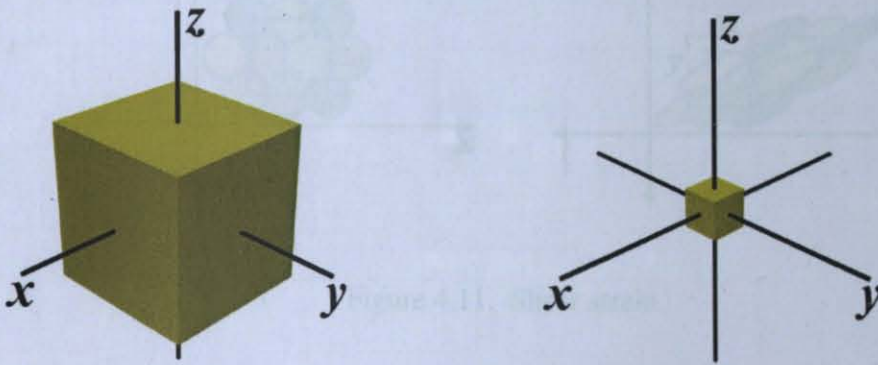


Figure 4.9. Volume Deformation (dilation)

**4.2.2.3. Rotational Deformation:** Angular Strain( $\psi$ ) show the rotational change. That is change in angle between 2 initially perpendicular lines. Angular shear is dimensionless. (Figure 4.10.)

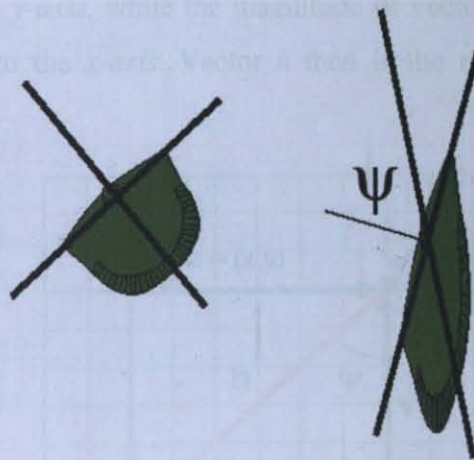


Figure 4.10. Angular strain

**Shear Strain ( $\gamma$ ):** The shear strain is defined in terms of the changes in angle of lines that were at right angles before deformation. The change of angle is  $\psi$  and the shear strain is  $\gamma$ . Shear strain is dimensionless (Figure 4.11.).

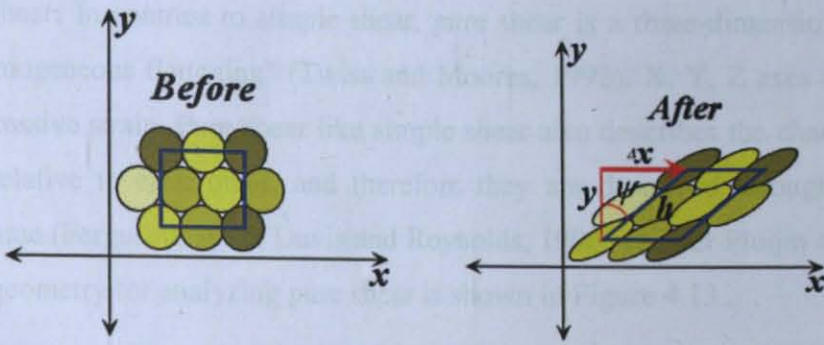


Figure 4.11. Shear strain

Simple Shear: Simple shear is a three-dimensional constant-volume strain (Twiss and Moores, 1992; Ferguson, 1994; Davis and Reynolds, 1996). It describes the change of points in a body relative to each other, and therefore they are described through an internal reference frame (Ferguson, 1994; Davis and Reynolds, 1996; van der Pluijm and Marshak, 1997). Involves a change in orientation of material lines along two of the principal axes ( $\lambda_1$  and  $\lambda_3$ ).

At the Figure 4.12., the magnitude of vector  $v$  is the distance that the point was translated parallel to the  $y$ -axis, while the magnitude of vector  $u$  is the distance the point was translated parallel to the  $x$ -axis. Vector  $h$  then is the resultant of these two vector components.

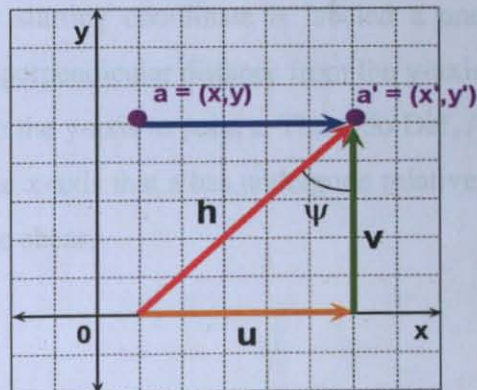


Figure 4.12. Simple shear

**Pure Shear:** In contrast to simple shear, pure shear is a three-dimensional constant-volume "homogeneous flattening" (Twiss and Moores, 1992). X, Y, Z axes do not rotate during progressive strain. Pure shear like simple shear also describes the change of points in a body relative to each other, and therefore they are described through an internal reference frame (Ferguson, 1994; Davis and Reynolds, 1996; van der Pluijm and Marshak, 1997). The geometry for analyzing pure shear is shown in Figure 4.13.,

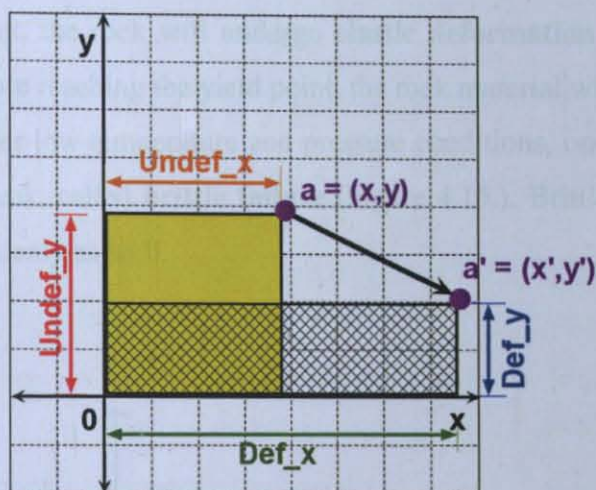


Figure 4.13. The translation of point  $a$  is used to illustrate the mathematics of pure shear.

On Figure 4.13., the starting coordinate is labeled  $a$  and during pure shear it is translated to  $a'$ .  $Def_x$  is the perpendicular distance from the  $y$ -axis to point  $a'$ .  $Undef_x$  is the perpendicular distance from the  $y$ -axis to point  $a$ . The ratio  $Def_x/Undef_x$  is the proportional change in position along the  $x$ -axis that  $a$  has undergone relative to its original position as it was translated during pure shear.

### 4.3. Relationship between Stress and Strain

Rocks behave in a variety of ways when stress is imposed on them. The relationship between stress and deformation is shown in stress-strain diagrams like those below. The reaction of rock material to an imposed stress depends on the temperature and pressure conditions. As stress is imposed on rock it starts to deform up to its **yield point**. Before it gets to the yield point, the rock will undergo **elastic deformation** (Figure 4.14.). If the stress is released before reaching the yield point, the rock material will return to its original shape. However, under low temperature and pressure conditions, once the rock reaches its yield point it will break, called **brittle failure** (Figure 4.15.). Brittle failure may occur if stress is imposed suddenly as well.

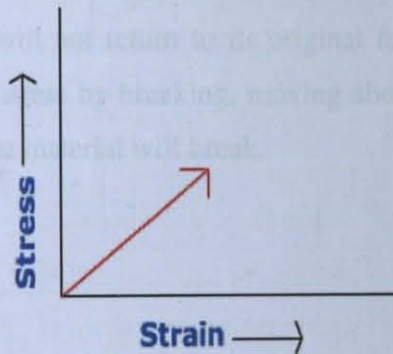


Figure 4.14. Elastic Deformation

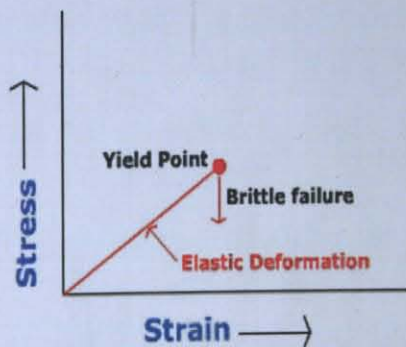


Figure 4.15. Brittle Failure

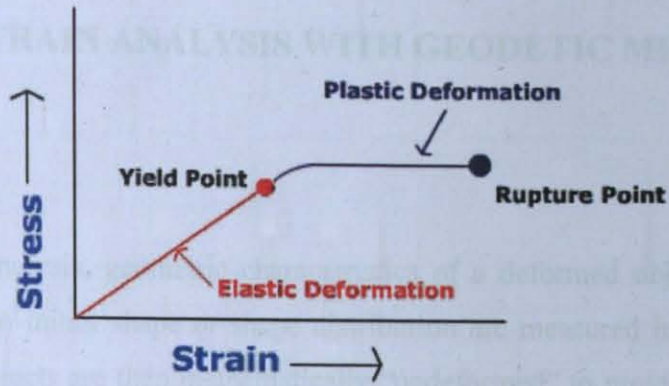


Figure 4.16. Plastic Deformation

Upon reaching the yield point under high pressure and temperature conditions, the rock may undergo **plastic deformation** (Figure 4.16.). In this case, once the rock changes shape and if stress is released, it will not return to its original form. During plastic deformation mineral bonds adjust to the stress by breaking, moving about, and then reforming. Once it reaches its **rupture point**, the material will break.

## 5. STRAIN ANALYSIS WITH GEODETIC METHODS

In strain analysis, geometric characteristics of a deformed object or population of objects of known initial shape or shape distribution are measured in the deformed state. The object or objects are then mathematically “undeformed” to provide a measurement of the amount of strain that object or population of objects has undergone.

In order to measure strain, we need to find objects in a deformed rock of known initial shape. While the original shape of objects is often known, the original size is usually unknown. Therefore, it is usually impossible to determine volumetric strain through strain analysis, and the focus is generally on distortional strain.

The procedure of strain analysis can be thought of as unraveling the effects of the combining two ellipsoids: the primary shape ellipsoid and the strain ellipsoid. These combine to form the final ellipsoid recorded in the rock.

Strain analysis are commonly used for determination of the deformation. The main geodetic methods that are used for strain accumulation are;

- adjusted measurements that is; length, angle and azimuth differences,
- coordinate differences,
- determination of strain parameters in an adjustment model.

Either of these methods are advantageous or disadvantageous can change according to the need of concerned problem. For the determination of these requirements, the strain parameters and their foregone size and their accuracy has great importance (Demir C.1999).

Table 5.1. Strain parameters that are defined by repeated geodetic observations

Parameters	Length	Azimuth	Angle	GPS
Area Deformation ( $\Delta$ )	+			+
Shear Strain ( $\gamma$ )	+	+	+	+
Eigenvalues ( $\epsilon_1, \epsilon_2$ )	+			+
Rotation Angle ( $\phi$ )	+	+	+	+
Angular Strain ( $\omega$ )		+		+

When we look at the table 5.1. the following results can be determined:

- Angle observations are enough to define shear strain and rotation of maximum shear.
- Besides angle observation, if azimuth measurement is done, then angular shear can be defined.
- Together with length measurements and area deformation, the parameters of symmetric strain tensor can be defined.
- The base line vectors that derived from GPS require scale and rotation parameters. By these measurements all the strain parameters can be determined.

### 5.1. Methods and Horizontal Strain Rate Distribution

Earth crust takes its shape from many small and large plates. It is known that these plates move according to each other. It is very important to search the movement characteristic of these plates. Recent years, researchers make a lot of research on the movement and rotate proportions of the plates. Moreover, strains on the plate boundaries and inside the plates have started to be determined.

Plate movements and the deformations and strain as a result of the movements can be defined by geological and geodetic methods. Since the observations take less time by geodetic methods, they are preferred. It is expected that, the comparisons of the results from two methods have to be close to each other.

The permanent observations on the geodetic network are beneficial for strain measurements. For this purpose it has to be assumed that;

- The geodetic network shows the characteristic features of the region,
- It is assumed that, the strains between permanent observations are homogenous and linear.

According to the above approach lots of models have developed. These are;

- a) The methods based on the strains that are infinitesimal,
- b) The determination of strain by finite element method.

Since the finite element method has developed recently and has limited applications, the infinitesimal strain model was used in this study.

### 5.1.1. Discrete triangle method

Under the assumption of uniform infinitesimal strain, the horizontal strain components can be calculated by the horizontal displacements of three points of a triangle. Supposing the displacements of the three points to be  $A : (u_A, v_A)$ ,  $B : (u_B, v_B)$ , and  $C : (u_C, v_C)$ , then the strain components can be calculated by (Eringen, 1980):

$$u_B - u_A = \Delta x_{AB} \epsilon_{xx} + \Delta y_{AB} \epsilon_{xy} + \Delta y_{AB} \omega \quad (5.1)$$

$$vB - vA = \Delta x_{AB} e_{xy} + \Delta y_{AB} e_{yy} - \Delta x_{AB} \omega \quad (5.2)$$

$$uC - uA = \Delta x_{AC} e_{xx} + \Delta y_{AC} e_{xy} + \Delta y_{AC} \omega \quad (5.3)$$

$$vC - vA = \Delta x_{AC} e_{xy} + \Delta y_{AC} e_{yy} - \Delta x_{AC} \omega \quad (5.4)$$

where  $\Delta x_{AB}$ ,  $\Delta y_{AB}$ ,  $\Delta x_{AC}$ , and  $\Delta y_{AC}$  are coordinate increments of sides AB and AC, respectively,  $\varepsilon_{xx}$ ,  $\varepsilon_{xy}$ , and  $\varepsilon_{yy}$  are the three components of the plane strain tensor, and  $\omega$  is the differential rotation (clockwise rotation is positive).

They are defined as:

$$\varepsilon_{xx} = \frac{\partial u}{\partial x} \quad (5.5)$$

$$\varepsilon_{yy} = \frac{\partial v}{\partial y} \quad (5.6)$$

$$\varepsilon_{xy} = \frac{1}{2} \left( \frac{\partial u}{\partial y} + \frac{\partial v}{\partial x} \right) \quad (5.7)$$

$$\omega = \frac{1}{2} \left( \frac{\partial u}{\partial y} - \frac{\partial v}{\partial x} \right) \quad (5.8)$$

where  $u$  is the displacement in  $x$  direction and  $v$  is the displacement in  $y$  direction. As long as the three points A, B, and C are not on a line, there is a unique solution. Noting that;

$$d = [ uB - uA \quad vB - vA \quad uC - uA \quad vC - vA ]^T \quad (5.9)$$

$$x = [ \varepsilon_{xx} \quad \varepsilon_{yy} \quad \varepsilon_{xy} \quad \omega ]^T \quad (5.10)$$

then it can be written as a matrix:

$$A * x = d \quad (5.11)$$

where

$$A = \begin{bmatrix} \Delta x_{AB} & 0 & \Delta y_{AB} & \Delta y_{AB} \\ 0 & \Delta y_{AB} & \Delta x_{AB} & -\Delta x_{AB} \\ \Delta x_{AC} & 0 & \Delta y_{AC} & \Delta y_{AC} \\ 0 & \Delta y_{AC} & \Delta x_{AC} & -\Delta x_{AC} \end{bmatrix} \quad (5.12)$$

### 5.1.2. Coordinate Differences:

$\Delta x$  and  $\Delta y$  coordinate differences can be measured according to the deformation analysis of a geodetic network or can be measured from periodical measurements on the adjusted network.

According to the local uniform deformation, these coordinate differences or deformation vektors can be defined as;

$$dx_i = x_i e_{xx} + y_i e_{xy} + t_x \quad (5.13)$$

$$dy_i = x_i e_{yx} + y_i e_{yy} + t_y \quad (5.14)$$

It can be shown by matrix as;

$$\begin{bmatrix} d_x \\ d_y \end{bmatrix} = \begin{bmatrix} 1 & 0 & x & y & 0 & 0 \\ 0 & 1 & 0 & 0 & x & y \end{bmatrix} \begin{bmatrix} t_x \\ t_y \\ e_{xx} \\ e_{xy} \\ e_{yx} \\ e_{yy} \end{bmatrix} \quad (5.15)$$

## 6. STRAIN ANALYSIS

### 6.1. Strain Tensor

Normal strain is the change in length in a given direction divided by the initial length in that direction. Shear strain is the complement of the angle between two initially perpendicular line segments. If a force is applied to a solid object, it may end up simultaneously translating, rotating and deforming the object.

Strain tensor can be defined by below matrix;

$$E = \begin{bmatrix} e_{xx} & e_{xy} \\ e_{xy} & e_{yy} \end{bmatrix} \quad (6.1)$$

The diagonal elements of strain tensor ( $e_{xx}$   $e_{yy}$ ) shows extension through the coordinate axes. The other elements ( $e_{xy}$ ) show the angular deformation that is a result from deformation according to coordinate axes.

Strain tensor parameters are determined with least square adjustment method. For strain parameters the below formulas are used:

Maximum strain:

$$\varepsilon_{\max} = \frac{1}{2} \left[ (e_{xx} + e_{yy}) + \sqrt{(e_{xx} - e_{yy})^2 + 4e_{xy}^2} \right] \quad (6.2)$$

Minimum strain:

$$\varepsilon_{\min} = \frac{1}{2} \left[ (e_{xx} + e_{yy}) - \sqrt{(e_{xx} - e_{yy})^2 + 4e_{xy}^2} \right] \quad (6.3)$$

Pure shear:

$$\gamma_2 = 2e_{xy} \quad (6.4)$$

$$\varphi = 0.5 * \tan^{-1} (\gamma_2 / \gamma_1) \quad (6.5)$$

Engineering shear:

$$\gamma_2 = 2e_{xy} \quad (6.6)$$

Maximum strain direction:

$$\varphi = 0.5 * \tan^{-1} (\gamma_2 / \gamma_1) \quad (6.7)$$

For the general definition of 3D Strain it can be said that; as in the one dimensional strain derivation, suppose that point  $P$  in a body shifts to point  $P'$  after deformation.

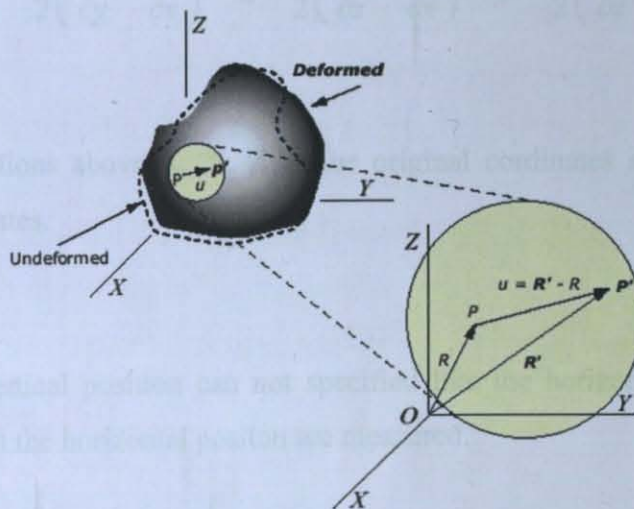


Figure 6.1. 3D Strain Figure

The infinitesimal strain-displacement relationships can be summarized as,

$$\varepsilon_{ij} = \frac{1}{2} \left( \frac{\partial u_i}{\partial x_j} + \frac{\partial u_j}{\partial x_i} \right) \quad (6.8)$$

where  $\mathbf{u}$  is the displacement vector,  $x$  is coordinate, and the two indices  $i$  and  $j$  can range over the three coordinates  $\{1, 2, 3\}$  in three dimensional space.

There are a total of 6 strain measures in a 3D strain tensor. These 6 measures can be organized into a matrix shown here,

$$\mathbf{e} = \begin{bmatrix} e_{xx} & e_{xy} & e_{xz} \\ e_{xy} & e_{yy} & e_{yz} \\ e_{xz} & e_{yz} & e_{zz} \end{bmatrix} \quad (6.9)$$

$$e_{xx} = \frac{\partial x'}{\partial x}, \quad e_{yy} = \frac{\partial y'}{\partial y}, \quad e_{zz} = \frac{\partial z'}{\partial z} \quad (6.10)$$

$$e_{xy} = \frac{1}{2} \left( \frac{\partial x'}{\partial y} + \frac{\partial y'}{\partial x} \right), \quad e_{xz} = \frac{1}{2} \left( \frac{\partial x'}{\partial z} + \frac{\partial z'}{\partial x} \right), \quad e_{yz} = \frac{1}{2} \left( \frac{\partial y'}{\partial z} + \frac{\partial z'}{\partial y} \right) \quad (6.11)$$

At the equations above  $X, Y, Z$  define original coordinates and  $X', Y', Z'$  define deformed coordinates.

Since the vertical position can not specified like the horizontal position accuracy, generally strains at the horizontal position are measured.

## 6.2. Strain Ellipse

In case of homogeneous strain, particles lying on a circle in the undeformed state, will lie on an ellipse in the deformed state and this ellipse is called strain ellipse (Figure 6.2.). Strain ellipse shows the strain parameters ( $\epsilon_{\max}$ ,  $\epsilon_{\min}$ ) that defines the maximum and minimum length deformation and their directions.

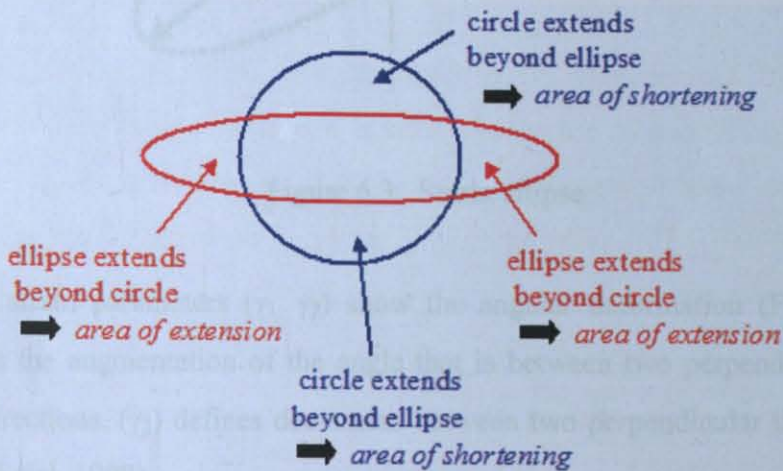


Figure 6.2. Strain ellipse

Strain parameters ( $\epsilon_{\max}$ ,  $\epsilon_{\min}$ ) can have positive and negative values. Positive values define extension and negative values define compression at the concerned area. If both strain parameters are positive, then they can be defined as strain ellipse. If strain parameters have positive and negative values then it can be shown with a two part hyperbola, and if both parameters are negative, then it can be defined with a virtual ellipse. On the graphical staging, positive and negative axis are shown with different character and the direction of extension is shown from point to the out, compression is defined vice versa (Vanicek et al, 1981).

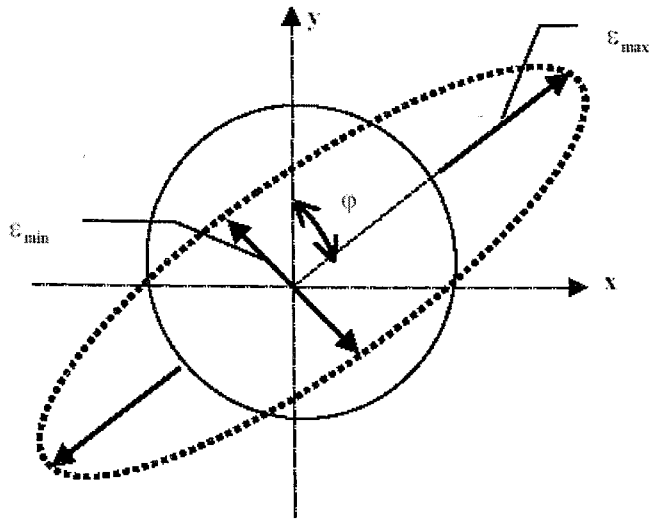


Figure 6.3. Strain ellipse

Shear strain parameters ( $\gamma_1$ ,  $\gamma_2$ ) show the angular deformation (Figure 6.4.). Pure shear ( $\gamma_1$ ) is the augmentation of the angle that is between two perpendicular northwest-northeast directions. ( $\gamma_2$ ) defines decrement between two perpendicular the north and east directions (Feigl, 1990).

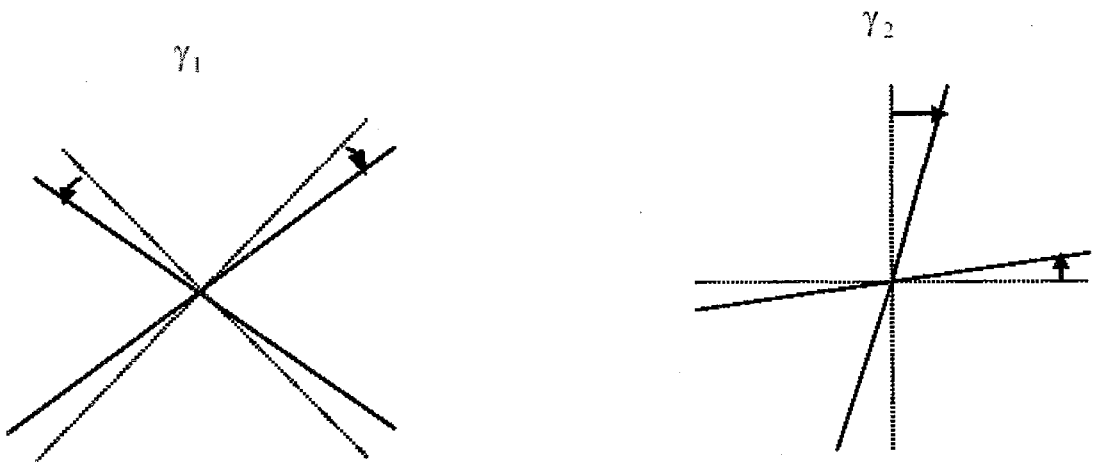


Figure 6.4. Shear strain parameters ( $\gamma_1$ ,  $\gamma_2$ ).

## 7. DETERMINATION OF STRAIN FIELD IN THE WESTERN PART OF NORTH ANATOLIAN FAULT ZONE

### 7.1. Computation of Strain Parameters with Triangulation

For this method the field was separated to six triangles and strain fields of all triangles assumed homogeneous and the strain parameters of each triangle was calculated (Table 7.1.). These parameters of strain tensor are the strain parameters of the point of equilibration of each triangle. For construction of triangles NETCAD software was used (Figure 7.1.).

Table 7.1. Strain fields

Regions	Point Names
Whole area	AVCT, BAD1, ULUT, BOZT, KART, MER1, MADT
Triangle 1	BAD1-BOZT-ULUT
Triangle 2	BAD1-BOZT-AVCT
Triangle 3	BOZT-ULUT-KART
Triangle 4	BOZT-AVCT-KART
Triangle 5	MER1-AVCT-KART
Triangle 6	MER1-MADT-KART

Triangles in the network are taken as “unit particle” of finite element method. By combining unit particles continuous parameter in the network (solution area), continuous parameters are found. For each baseline of a triangle, three general equations are created. Thus,  $e_{xx}$ ,  $e_{xy}$ ,  $e_{yy}$  are found.

Strain parameters which were calculated with this method are independent from datum parameters. Calculated strain parameters for the points of equilibration of triangles

show scale differences in the network. It is required to provide the continuity for the network among the parameters which are calculated for points of equilibration.

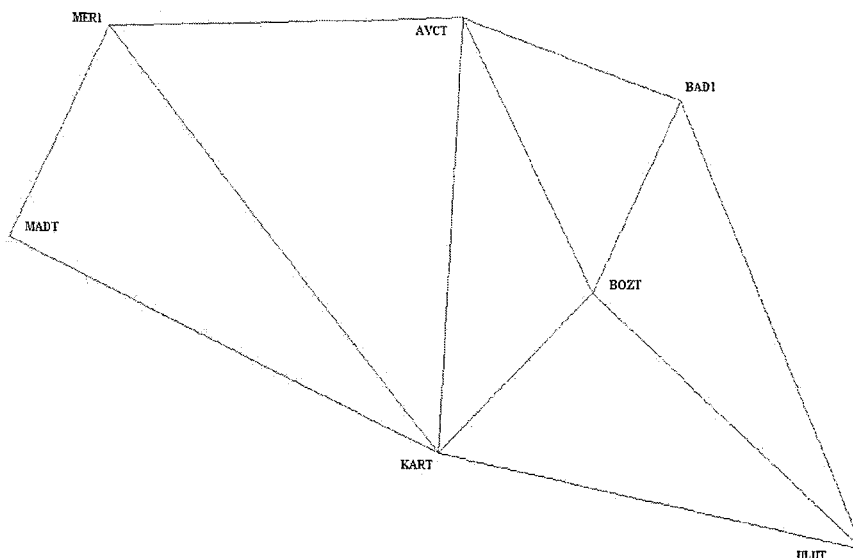


Figure 7.1. Triangles of the field

An example of the computation of strain parameters (Table 7.2) for a triangle was given below related to Figure 7.1.

Table 7.2a. Strain tensor parameters from triangulation

STATION ID	2002		2004	
	North (m)	East (m)	North (m)	East (m)
MER1	4537346,6215	580957,8216	4537346,6508	580957,8839
MADT	4497579,4590	549671,5361	4497579,4702	549671,5348
KART	4459834,6113	613353,0304	4459834,6232	613353,0363

Table 7.2b. Strain tensor parameters from triangulation

Baseline	$\Delta X$	$\Delta Y$	$\Delta X$	$\Delta Y$
MER1-MADT	39767,1625	31286,2855	39767,1806	31286,3491
MER1-KART	77512,0102	-32395,2088	77512,0276	-32395,1524
MADT-KART	37744,8477	-63681,4943	37744,8470	-63681,5015

Side Lengths:

$$\begin{aligned} S_{12} &= 50599,0007\text{m} & S'_{12} &= 50599,0543\text{m} \\ S_{13} &= 84009,2928\text{m} & S'_{13} &= 84009,2871\text{m} \\ S_{23} &= 74027,0643\text{m} & S'_{23} &= 74027,0701\text{m} \end{aligned}$$

Side Length Differences:

$$\begin{aligned} \Delta S_{12} &= 0,0535\text{m} \\ \Delta S_{13} &= -0,0057\text{m} \\ \Delta S_{23} &= 0,0058\text{m} \end{aligned}$$

$$\begin{aligned} e_{12} &= 1,0583\mu s & e_{13} &= -0,0678\mu s & e_{23} &= 0,0788\mu s \\ e_{12} &= 1,0583 & e_{13} &= -0,0678 & e_{23} &= 0,0788 \\ \alpha_{12} &= 42^{\circ}, 4371 & \alpha_{13} &= 174^{\circ}, 7978 & \alpha_{23} &= 134^{\circ}, 0620 \end{aligned}$$

$$\varepsilon = e_{xx} \cos^2 t + e_{xy} \sin 2t + e_{yy} \sin^2 t \quad (7.1)$$

$$A = \begin{bmatrix} 0,3823 & 0,9719 & 0,6177 \\ 0,1487 & -0,7116 & 0,8513 \\ 0,7400 & -0,8772 & 0,2600 \end{bmatrix}$$

$$l = \begin{bmatrix} 1,0583 \\ -0,0678 \\ 0,0788 \end{bmatrix}$$

$$x = \begin{bmatrix} e_{yy} \\ e_{xy} \\ e_{xx} \end{bmatrix} = \begin{bmatrix} 0,3692 \\ 0,2322 \\ 0,0883 \end{bmatrix}$$

$$x = (A^T A)^{-1} A^T l \quad (7.2)$$

$$E_1 = 0,50\mu s$$

$$E_2 = 0,04\mu s$$

$$\beta = 45^{\circ}, 46$$

$$E_{SHEAR} = 0,27\mu s$$

$$E_{INTER} = 0,23\mu s$$

After computation of strain tensor parameters, maksimum and minimum principle strain components were calculated (Table 7.3.). These values were put on the GMT

computer program to show the extension or compression of the areas. The arrows were put on the equilibration of triangles.

Table 7.3. Calculated strain parameters

TRIANGLE CORNER POINTS	PRINCIPLE STRAIN COMPONENTS		$\Psi$ (deg)	$E_{INTER}$ ( $\mu s$ )	$E_{SHEAR}$ ( $\mu s$ )
	$\epsilon_1$ ( $\mu s$ )	$\epsilon_2$ ( $\mu s$ )			
BAD1-BOZT-ULUT	0,5828	-0,0859	6,9826	0,2485	0,3344
BAD1-BOZT-AVCT	0,7782	-0,3067	30,9725	0,2357	0,5425
BOZT-ULUT-KART	0,2189	-0,5221	-89,9999	-0,1516	0,3705
BOZT-AVCT-KART	0,4077	-1,395	47,9029	-0,4935	0,9012
MER1-AVCT-KART	0,4102	-0,075	54,0592	0,1676	0,2425
MER1-MADT-KART	0,5001	-0,0426	40,9145	0,2287	0,2714

Figure 7.2 shows the extension of the area that is formed from BAD1 (Buyukada), BOZT (Bozburun) and ULUT (Uludag) triangles.

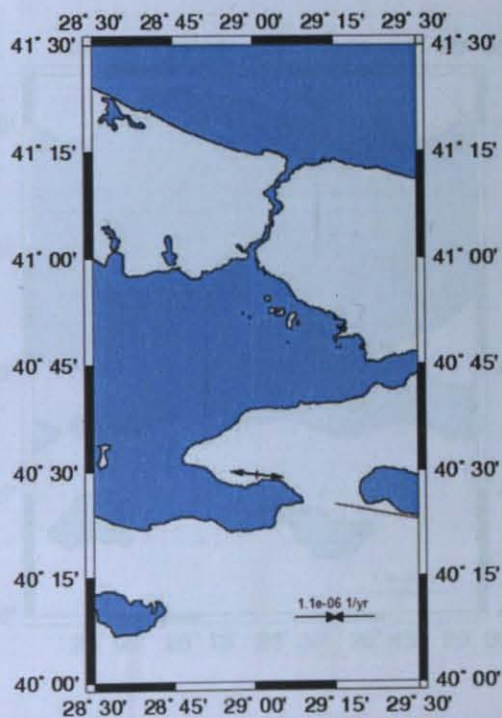


Figure 7.2. Extensions and compressions accepted as homogeneous in the MER1-AVCT-KART

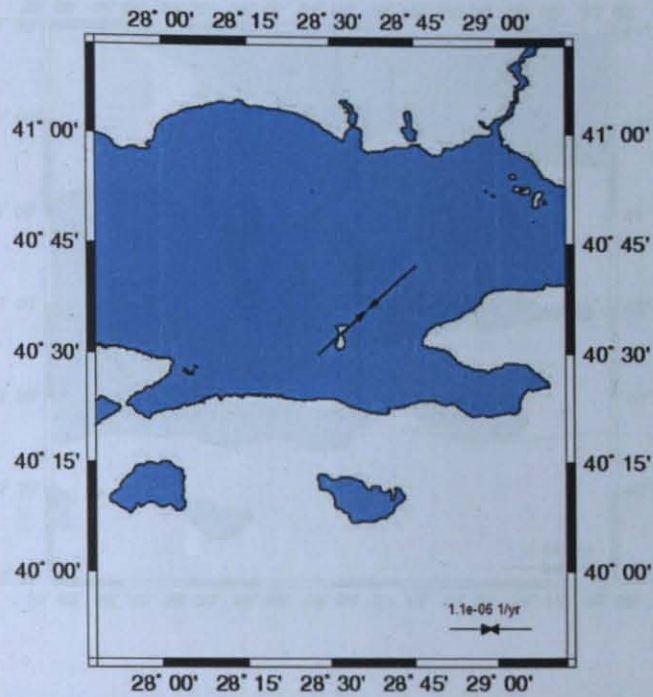


Figure 7.3 shows the compression at the AVCT (Avcilar), KART (Karacabey) and BOZT (Bozburun) triangle.

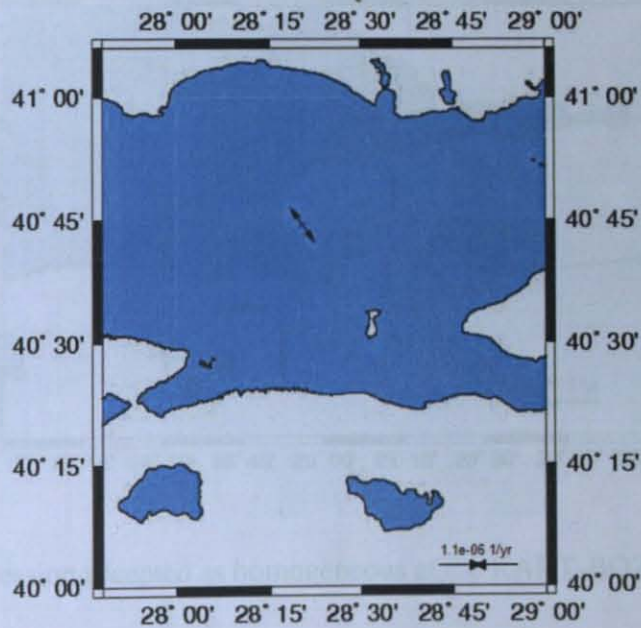


Figure 7.4. Extensions and compressions accepted as homogeneous in the MER1-AVCT-KART triangle.

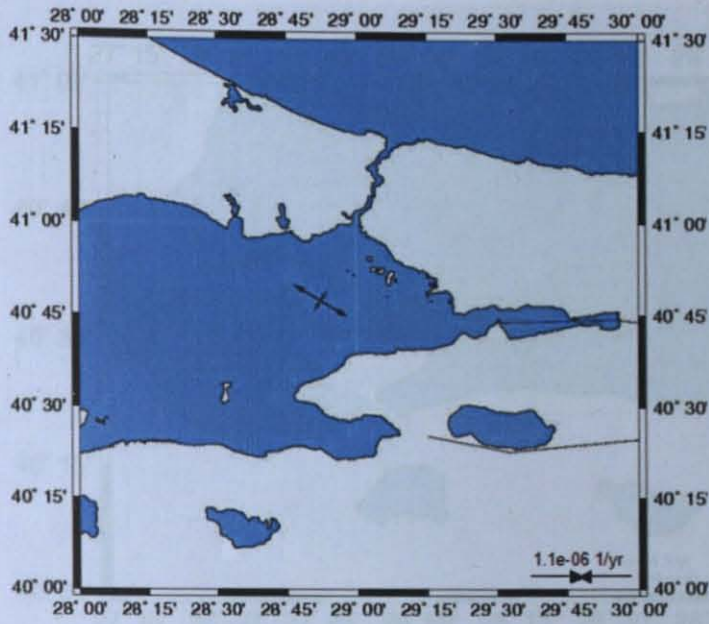


Figure 7.5. Extensions and compressions accepted as homogeneous at the BOZT-AVCT-BAD1 triangle.

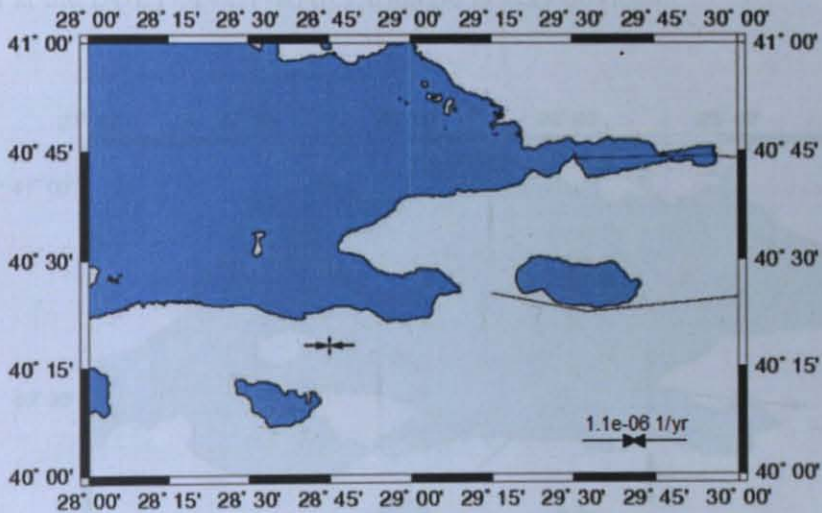


Figure 7.6. Compression accepted as homogeneous at the KART-BOZT-ULUT triangle.

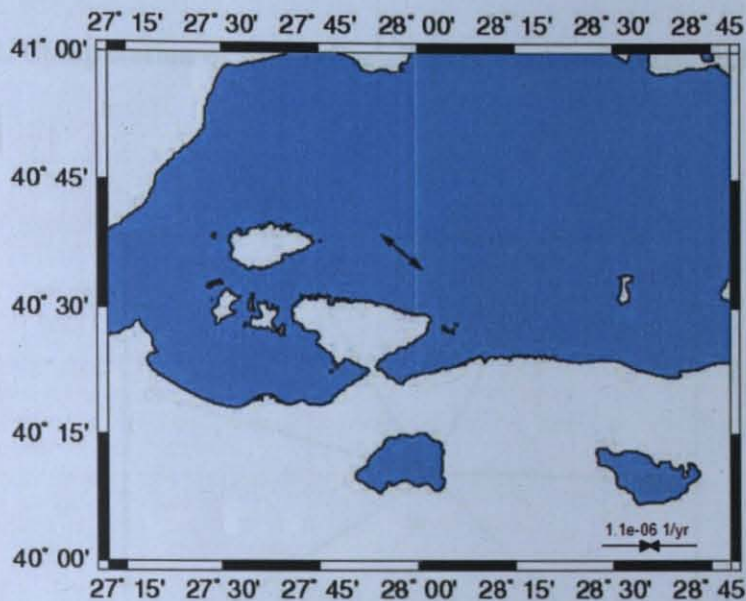


Figure 7.7. Extension accepted as homogeneous at the KART-MER1-MADT triangle

Figure 7.7. Extension accepted as homogeneous at the KART-MER1-MADT triangle

For the whole area, the compression and extension can be seen at the figure 7.8. The compression at the BOZT-AVCT-KART triangle is very obvious.

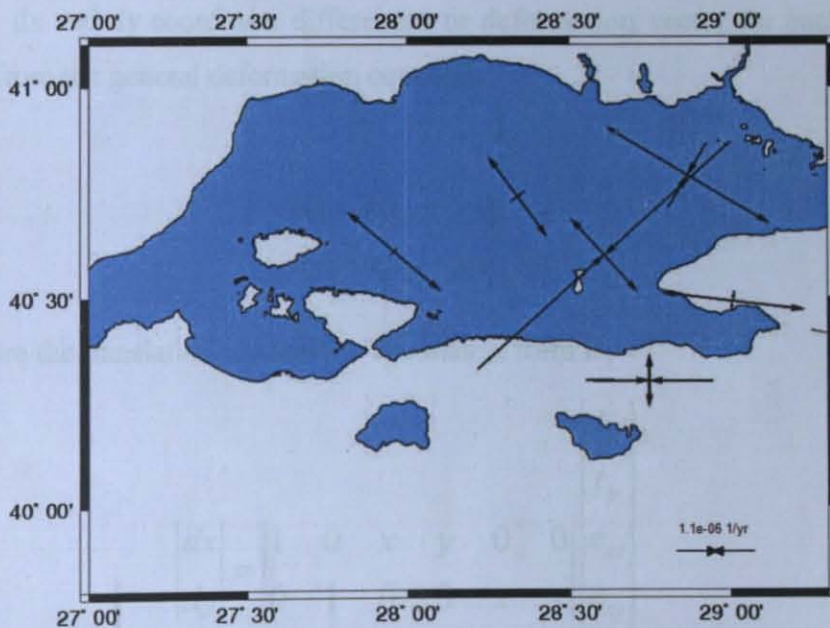


Figure 7.8. Extensions and compressions for whole region accepted as homogeneous

## 7.2. Computation of Strain Parameters with Infinitesimal Method

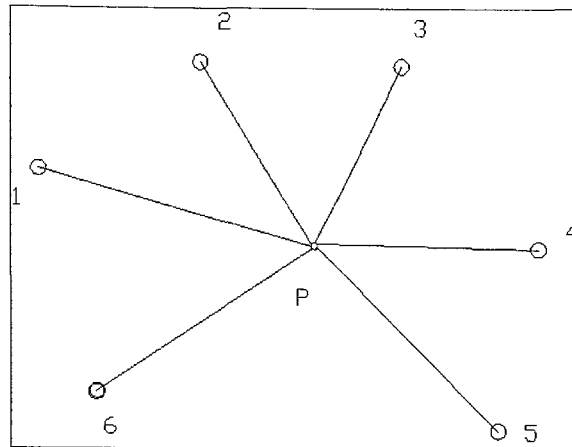


Figure 7.9. Point P and its surrounding points

This method is based on the measurements coordinate differences between a fixed point and its surroundings. Strain tensor parameters are calculated from adjusted coordinate differences. This method can be applied if the number of connections are more than three.  $dx$  and  $dy$  coordinate differences or deformation vector for each point can be measured from the general deformation equation.

$$dx_i = x_i e_{xx} + y_i e_{xy} + t_x \quad (7.3)$$

$$dy_i = x_i e_{yx} + y_i e_{yy} + t_y \quad (7.4)$$

$t_x$ ,  $t_y$  are the translation unknowns. The matrix form is;

$$\begin{vmatrix} dx \\ dy \end{vmatrix} = \begin{vmatrix} 1 & 0 & x & y & 0 & 0 \\ 0 & 1 & 0 & 0 & x & y \end{vmatrix} \begin{vmatrix} t_x \\ t_y \\ e_{xx} \\ e_{xy} \\ e_{yx} \\ e_{yy} \end{vmatrix} \quad (7.5)$$

The equations above are valid for every point that are connected to a P point in a geodetic network. Thus, the equation can be extended as;

$$x = X_i - X_p \quad (7.6)$$

$$y = Y_i - Y_p \quad i=1, \dots, n \quad (7.7)$$

There are 6 unknown at the above equations. Firsts two of them are translations and last four of them are the strain tensor parameters. These parameters of strain tensor are the strain parameters of any particular point (P). Then, strain parameters are calculated from the parameters of strain tensor.

$$\Delta = e_{xx} + e_{yy} \quad (7.8)$$

$$\gamma_1 = e_{xx} - e_{yy} \quad (7.9)$$

$$\gamma_2 = 2e_{xy} \quad (7.10)$$

$$\gamma = \sqrt{\gamma_1^2 + \gamma_2^2} \quad (7.11)$$

where  $\Delta$  is dilation,

$\gamma_1$  is principal shear strain,

$\gamma_2$  is engineering shear strain,

$\gamma$  is total shear strain.

Principal strain parameters are;

$$E_1 = \frac{1}{2}(\Delta + \gamma) \quad (7.12)$$

$$E_2 = \frac{1}{2}(\Delta - \gamma) \quad (7.13)$$

$$\beta = \arctan \left( \frac{e_{xy}}{E_1 - e_{xy}} \right) \quad (7.14)$$

where  $E_1$  is maximum principal strain,

$E_2$  is minimum principal strain,

$\beta$  is direction of maximum principal strain arc.

Maximum shear strain;

$$E_{SHEAR} = 0,5(E_1 - E_2) \quad (7.15)$$

Maximum normal strain

$$E_{INTER} = 0,5(E_1 + E_2) \quad (7.16)$$

Strain parameters which are calculated from baseline or coordinates differences between two epochs give strain accumulation. If these values are divided by time interval between two epochs  $\Delta t$ , strain rate is obtained.

Table 7.4. Coordinate differences for infinitesimal homogeneous model calculation

STATION ID	2002		2004		Differences	
	North (m)	East (m)	North (m)	East (m)	N (m)	E (m)
KART	4459834,6113	613353,0304	4459834,6232	613353,0363	0,0119	0,0059
MER1	4537346,6215	580957,8216	4537346,6508	580957,8839	0,0293	0,0623
AVCT	4540746,2518	645065,1751	4540746,2100	645065,1897	-0,0418	0,0146
BOZT	4490393,2793	650985,7629	4490393,2910	650985,7728	0,0117	0,0099
ULUT	4442538,4509	681760,1983	4442538,4621	681760,1988	0,0112	0,0005
BAD1	4526310,0902	678593,2138	4526310,1070	678593,2521	0,0168	0,0383

The coordinate differences of stations between two years stations were calculated for "I" matrix (Table 7.4.). For matrix A the differences of all points from a fixed point were computed and they formed the matrix A.

$$A = \begin{bmatrix} 1 & 0 & 37744,8477 & -63681,4943 & 0 & 0 \\ 0 & 1 & 0 & 0 & 37744,8477 & -63681,4943 \\ 1 & 0 & 77512,0102 & -32395,2088 & 0 & 0 \\ 0 & 1 & 0 & 0 & 77512,0102 & -32395,2088 \\ 1 & 0 & 80911,6405 & 31712,1447 & 0 & 0 \\ 0 & 1 & 0 & 0 & 80911,6405 & 31712,1447 \\ 1 & 0 & 30558,6680 & 37632,7325 & 0 & 0 \\ 0 & 1 & 0 & 0 & 30558,6680 & 37632,7325 \\ 1 & 0 & -17296,1604 & 68407,1679 & 0 & 0 \\ 0 & 1 & 0 & 0 & -17296,1604 & 68407,1679 \\ 1 & 0 & 0 & 0 & 0 & 0 \\ 0 & 1 & 0 & 0 & 0 & 0 \end{bmatrix}$$

$$I = \begin{bmatrix} 0,0112 \\ -0,0013 \\ 0,0293 \\ 0,0623 \\ -0,0418 \\ 0,0146 \\ 0,0117 \\ 0,0099 \\ 0,0112 \\ 0,0005 \\ 0,0119 \\ 0,0059 \end{bmatrix} \quad x = (A^T * A)^{-1} A^T * I = \begin{bmatrix} 0,019805824 \\ 0,002389661 \\ -3,51319E-07 \\ -2,82132E-07 \\ 3,74789E-07 \\ -0,22327E-07 \end{bmatrix} = \begin{bmatrix} t_x \\ t_y \\ e_{xx} \\ e_{xy} \\ e_{yx} \\ e_{yy} \end{bmatrix}$$

Here, x matrix include two rotation parameter as  $t_x$  and  $t_y$ , and strain tensor parameters as  $e_{xx}$ ,  $e_{yy}$ ,  $e_{xy}$  and  $e_{yx}$ . With strain tensor parameters maksimum and minimum strain prnciple parameters and maksimum strain rotation can be calculated;

$$\varepsilon_1 = 0.5 * (e_{xx} + e_{yy}) + \sqrt{(0.25 * (e_{xx} + e_{yy})^2 + e_{xy}^2)} \quad (7.17)$$

$$\varepsilon_2 = 0.5 * (e_{xx} + e_{yy}) - \sqrt{(0.25 * (e_{xx} + e_{yy})^2 + e_{xy}^2)} \quad (7.18)$$

$$\beta = \arctan \frac{e_{xy}}{\varepsilon_1 - e_{xy}} \quad (7.19)$$

The results are;

$$E_1 = -0,16 \mu s$$

$$E_2 = -3,57 \mu s$$

$$\beta = 26^{\text{deg}}, 3721$$

This calculation was applied to all points which has baseline with at least three points. For that reason the station MADT was not included in the computation, since it has only two baselines. All results are shown at the Table 7.5.

Table 7.5. Infinitesimal strain parameters

STATION ID	Principle strain parameters		$\beta$ (deg)
	$\varepsilon_1$ ( $\mu s$ )	$\varepsilon_2$ ( $\mu s$ )	
KART	-0,16	-3,57	63,721
MER1	1,25	-0,48	48,121
AVCT	5,66	-0,31	53,968
BOZT	0,22	-0,08	23,227
ULUT	0,15	0,05	42,705
BAD1	0,70	-0,09	85,418

## 8. CONCLUSION

The Marmara sea region (NW Turkey) is a tectonically active region situated at the western end of the North Anatolian Fault zone (NAFZ) which splits into several branches in this region. During the last century there has been a westward migration of earthquakes along the NAFZ, and a large earthquake is expected in the Marmara sea in a near future. For that reason there has been many projects to obtain the information of the strain accumulation along fault lines and to determine the earthquake potential.

Before the 1999 earthquakes, the Marmara ContinuousGPSnetwork(MAGNET) was established to measure the deformations associated with strain accumulation along the western NAF system. After the 1999-earthquakes the network was extended to track the postseismic deformations caused by the earthquakes and to monitor the different fault systems in the Marmara region (Reilinger et al., 2000; Burgmann et al., 2002a, 2002b; Hearn et al., 2002; Ergintav et al., 2002).

At the western part of North Anatolian Fault (NAF) by using seven continuous GPS stations from MAGNET the annual movements and directions of the stations are determined. The calculated velocity field indicates systematic augmentation from south to north. The stations which are located northern part like AVCT, BAD1 and MER1 moves faster than the ones located at the southern part like BOZT, KART, MADT and ULUT. The reason of this faster movements is that; the stations at the northern part are closer to fault than the southern ones.

Since the Marmara Region shows tectonically active complex behaviour there hasn't been many studies related to determine strain accumulation. The limited studies define determination of strain accumulation of the whole area.

Since now, Marmara Region has been investigated by many scientists. At Demir C. study, the strain parameters were determined for the whole area by four different methods, as linear transformation to strain field from velocity field, finite element method, infinitesimal deformation method. After comparisons of these four methods, he figured out the wideness of deformation zone at the Anatolian and Eurasian plates through the NAF.

At his Phd thesis, Yilmaz O. compare the strain accumulation with two methods as infinitesimal strain rate model and linear transformation to stain field from velocity field. He figured that the southern branch of NAFZ between Iznik-Mekece has the smallest strain accumulation.

In this study, strain accumulation around the fault zones in western Marmara Region was calculated with two techniques as triangulation and infinitesimal strain model. Since the region has very complex tectonic characteristic, the strain parameters were calculated separately.  $\epsilon_1$  and  $\epsilon_2$  defines the principle strain parameters. Positive values of principle strain parameter refer extension, negative values refer compression. Figure 7.8 explains the strain accumulation of the whole region. As it is seen on the figure, arrows explain either extension of compression quantities. The size of arrows have different amounts. The reason of this difference is related with how close are the stations to fault and also to each other.

## REFERENCES

- Ambraseys, the earthquake of 10 July 1894 in the Gulf of Izmit (Turkey) and its relation to the earthquake of 17 August 1999, *J. Seismol.*, **5**, pp. 117–128, 2001.
- Barka, A. ve Kadinsky-Cade, K., , “Strike-Slip Fault Geometry in Turkey and its Influence on Earthquake Activity”, *Tectonics*, **7**, 663, 1988.
- Barka, A., ve Reilinger, R., “Active Tectonics of the Eastern Mediterranean Region: Deduced from GPS, Neotectonic and Seismicity Data”, *Ann. Geofis.*, **40**, pp. 587, 1997.
- Burgmann, R., Ayhan, M.E., Fielding, E.J., Wright, T. J., McClusky, S., Aktug, B., Demir, C., Lenk, O., Turkezer, A., “Deformation during the 12 November 1999 Duzce, Turkey Earthquake, from GPS and InSAR Data”. *Bulletin of the Seismological Society of America*, **92** (1), pp. 161, 2002.
- Demir, C., *Kuzey Anadolu Fay Zonu Bati Kesiminde Yatay Yer Kabugu Hareketleri ve Gerinim Birikiminin Arastirilmesi*, YTÜ, Fen Bilimleri Enstitüsü, Doktora Tezi, Istanbul, 1999.
- Demirel, H., *Dengeleme Hesabi*, Yıldız Technical University, 2003
- Deniz, R., Jeodezik Verilerden Strain Analizi, Jeodezi Anabilim Dalı Seminerleri, Istanbul Technical University, İstanbul, Turkey, 1997.
- Deniz, R., Jeodezik Ölçmelerden Yerkabuğundaki Lokal Gerilimlerin Belirlenmesi, *İTÜ Dergisi*, Vol:48, No:4, 1990.

- Denli, H., *GPS ile Marmara Bölgesindeki Yerkabuğu hareketlerinin belirlenmesi*, Ph.D. Thesis, Istanbul Technical University, Istanbul, Turkey, 1998.
- S. Ergintav, U. Dogan, C. Gerstenecker, R. Cakmak, A. Belgen, H. Demirel, C. Aydin, R. Reilinger, “A snapshot (2003–2005) of the 3D postseismic deformation for the 1999,  $M_w = 7.4$  Izmit earthquake in the Marmara Region, Turkey, by first results of joint gravity and GPS monitoring” *Journal of Geodynamics*, 2007.
- Feigl, K. L., King, R. W., Jordan, T. H., (), “Geodetic Measurement of Tectonic Deformation in the Santa Maria Fold and Thrust Belt, California”, *Journal of Geophysical Research*, Vol. 95, No. B3, pp. 2679, 1990.
- Kahle, H., Cocard, M., Peter, Y., Geiger, A., Reilinger, R. E., McClusky, S., King, R. W., Barka, A., Geis, G., “The GPS Strain Rate Field in the Aegean Sea and Western Anatolia”, *Geophysical Research Letter*, 26, pp. 2513, 1999.
- McClusky, S., Aktug, B., Aygul, H., Baassanian, S., Barka, A., Burchfiel, C., Cakmak, R., Ergintav, S., Hamburger, M., Kahle, H., Kastens, K., King, R., Kotzev, V., Mahmoud, S., Nadariya, M., Ozener, H., Prilepin, M., Reilinger, R., Seeger, H., Tari, E., Turkezer, A., Veis, G., “GPS Constraints on Active Tectonics in the Eastern Mediterranean Region”, UNAVCO Meeting, Boulder CO., April 7, 1999.
- McClusky, S., Balassanian, S., Barka, A., Demir C., Ergintav, S., Georgiev, I., Gurkan, O., Hamburger, M., Hurst, K., Kahle, K., Kastens, K., Kekelidze, G., King, R., Kotzev, V., Lenk, O., Mahmoud, S., Mishin, M., Nadariya, M., Ouzounis, A., Paradissis, D., Peter, Y., Prilepin, M., Reilinger, R., Sanli, I., Seeger, H., Tealeb, A., Toksöz, M.N., Veis, G., , ”Global Positioning System constrains on plate kinematics and dynamics in the eastern Mediterranean and Caucasus”, *Journal of Geophys. Res.*, Vol. 105, No. B3, pp. 5695–5719, 2000.
- R. Armijo, B. Meyer, S. Navarro, G. King, and A. Barka, Asymmetric slip partitioning in the Sea of Marmara pull-apart: A clue to propagation processes of the North Anatolian fault?, *Terra Nova*, 14, pp. 80–86, 2002.

- Reilinger, R. E., Ergintav, S.; Burgmann, R., McClusky, S., Lenk, O., Barka, A., Gürkan, O., Hearn, L., Feigl, K.L., Çakmak, R.; Aktug, B., Özener, H., Toksöz, M. N., “Coseismic and Postseismic Fault Slip for the 17 August 1999, M = 7.5, Izmit, Turkey Earthquake”, *Science*, Vol. 289, 2000
- Straub, C.; *Recent Crustal Deformation and Strain Accumulation in the Marmara Sea Region, N.W. Anatolia, Inferred from GPS Measurements*, PhD Thesis, ETH Zürich, Switzerland. 1996
- Tüysüz, O. ve Genç, C., “Geological Factors Controlling the Distribution of Damage During the 17<sup>th</sup> August and 12<sup>th</sup> November 1999 Earthquakes”, *International Conference on The Kocaeli Earthquake*, Kocaeli, 1999.
- Vanicek, P., Thapa, K. ve Schneider, D., “The Use of Strain to Identify Incompatible Observations and Constraints in Horizontal Geodetic Networks”, *Manuscripta Geodaetica*, 6, 257-281. 1981.
- Üçer, B., Eyidogan, H., Gürbüz, C., Barka, A., Serif, B., “Seismic Investigations of Marmara Region in Active Tectonics of Northwest Anatolia”, The Marmara Poly-Project, Hochschulverlag AG an der ETH, Zurich, pp. 55-87, 1997